Comparative cranial osteology of *Blanus* (Squamata: Amphisbaenia)

ANDREA VILLA[1,*], MARTIN KIRCHNER[2], DAVID M. ALBA[3], FEDERICO BERNARDINI[4,5], ARNAU BOLET[3,6], ÀNGEL H. LUJÁN[3,7], JOSEP FORTUNY[3,8], CHRISTY A. HIPSLEY[9,10], JOHANNES MÜLLER[2], ROBERTO SINDACO[11], CLAUDIO TUNIZ[5] AND MASSIMO DELFINO[1,3]

[1]*Dipartimento di Scienze della Terra, Università di Torino, Via Valperga Caluso 35, 10125 Torino, Italy*
[2]*Museum für Naturkunde, Leibniz Institute for Evolution and Biodiversity Science, 10115 Berlin, Germany*
[3]*Institut Català de Paleontologia Miquel Crusafont, Universitat Autònoma de Barcelona, Edifici ICTA-ICP, c/ Columnes s/n, Campus de la UAB, 08193 Cerdanyola del Vallès, Barcelona, Spain*
[4]*Centro Fermi, Museo Storico della Fisica e Centro di Studi e Ricerche 'Enrico Fermi', Piazza del Viminale 1, 00184 Roma, Italy*
[5]*Multidisciplinary Laboratory, the 'Abdus Salam' International Centre for Theoretical Physics, Via Beirut 31, 34151 Trieste, Italy*
[6]*School of Earth Sciences, University of Bristol, Life Sciences Building, 24 Tyndall Avenue, Bristol BS8 1TQ, UK*
[7]*Department of Geological Sciences, Faculty of Science, Masaryk University, Kotlářská 2, 611 37, Brno, Czech Republic*
[8]*Centre de Recherches sur la Paléobiodiversité et les Paléoenvironnements, Muséum National d'Histoire Naturelle, Bâtiment de Paléontologie, CP38, 8 rue Buffon, 75005 Paris, France*
[9]*School of BioSciences, University of Melbourne, Parkville, VIC 3010, Australia*
[10]*Museums Victoria, GPO Box 666, Melbourne, VIC 3001, Australia*
[11]*Museo Civico di Storia Naturale, via San Francesco di Sales 88, I-10022 Carmagnola, Italy*

Worm lizards, or amphisbaenians, of the genus *Blanus* are found in various countries around the Mediterranean Sea. In addition to four extinct species, seven extant taxa are currently recognized. Here, we present the first comparative analysis of the cranial osteology of *Blanus* including all extant species. The results of this analysis show a homogeneous morphology among skull bones, with few morphological features that can be used to discriminate among different *Blanus* species. No clear osteological diagnostic features can be identified for any single species. The most taxonomically significant bones are the premaxilla and the quadrate. In particular, the premaxillae can be used to discriminate perfectly between the two molecular-based clades into which extant blanids are currently separated. Despite the relatively similar skull morphology, detailed comparative osteological studies such as this one are useful to evaluate the phylogenetic affinities of extant and extinct taxa. The extinct *Blanus mendezi*, for example, recalls the western *Blanus* species in the morphology of the premaxilla and some of the eastern ones in the morphology of the quadrate. The inclusion of these features in future phylogenetic analyses will be of utmost importance to clarify the affinities of this and other *Blanus* species, both extinct and extant.

ADDITIONAL KEYWORDS: Blanidae – *Blanus alexandri* – *Blanus aporus* – *Blanus cinereus* – *Blanus mettetali* – *Blanus strauchi* – *Blanus tingitanus* – *Blanus vandellii* – comparative anatomy.

*Corresponding author. E-mail: a.villa@unito.it

INTRODUCTION

Amphisbaenians are squamate reptiles currently living in Central, South and North America, Africa, the Middle East and the Mediterranean region (Vitt & Caldwell, 2009). They all have a fossorial lifestyle and share a peculiar morphology, mainly characterized by an elongated body, loss of limbs (except *Bipes*) and a skull morphology adapted to burrowing habits. Six extant families and > 190 extant species are currently recognized (Uetz *et al.*, 2017). The affinities of amphisbaenians with other squamates (i.e. lizards and snakes) are still a matter of debate. Different positions in the squamate tree have been suggested (see, e.g. Conrad, 2008; Müller *et al.*, 2011; Gauthier *et al.*, 2012; Reeder *et al.*, 2015), but such positions might be strongly influenced by converging traits linked to fossoriality, at least in some cases (Müller *et al.*, 2016). Recent phylogenies recovered a sister-group relationship with lizards of the family Lacertidae (i.e. Müller *et al.*, 2011; Reeder *et al.*, 2015).

Figure 1. *Blanus alexandri*.

Blanus Wagler, 1830 (Fig. 1) is a Palaearctic genus of amphisbaenians from the family Blanidae. Members of *Blanus* currently live in Mediterranean countries of Europe, Northern Africa and the Middle East (Sindaco & Jeremčenko, 2008; Uetz *et al.*, 2017). Seven extant species are recognized (Uetz *et al.*, 2017): *Blanus cinereus* (Vandelli, 1797) and *Blanus vandellii* Ceríaco & Bauer, 2018 in the Iberian Peninsula; *Blanus mettetali* Bons, 1963 and *Blanus tingitanus* Busack, 1988 in Morocco; and *Blanus alexandri* Sindaco *et al.*, 2014, *Blanus aporus* Werner, 1898 and *Blanus strauchi* (Bedriaga, 1884) in southern Anatolia, Eastern Aegean Islands, Syria, Lebanon and northern Iraq. *Blanus mariae* Albert & Fernández, 2009 was described after the identification of two distinct genetic lineages in *B. cinereus*. The so-called 'central' Iberian clade was referred to *B. cinereus*, whereas the 'southern' Iberian clade was named *B. mariae*. Based on a misidentification of the type locality of *B. cinereus* by Albert & Fernández (2009), Ceríaco & Bauer (2018) recently demonstrated that the name *B. cinereus* should be used for the 'southern' clade, thereby considering that *B. mariae* is a junior synonym of the latter. They consequently provided a new name for the 'central' clade: *B. vandellii*. The fossil record of *Blanus* is extensive and consists of four extinct species: *Blanus antiquus* Schleich, 1985, *Blanus gracilis* (Roček, 1984), *Blanus mendezi* Bolet *et al.*, 2014 and *Blanus thomaskelleri* Čerňanský *et al.*, 2015b. Based on molecular analyses (Sindaco *et al.*, 2014; Sampaio *et al.*, 2015), two extant clades can be recognized, in further agreement with their disjunct geographical distribution (Fig. 2): one including *B. cinereus*, *B. vandellii*, *B. mettetali* and *B. tingitanus* (Western Group) and another composed by *B. alexandri*, *B. aporus* and *B. strauchi* (*B. strauchi* complex, or Eastern Group).
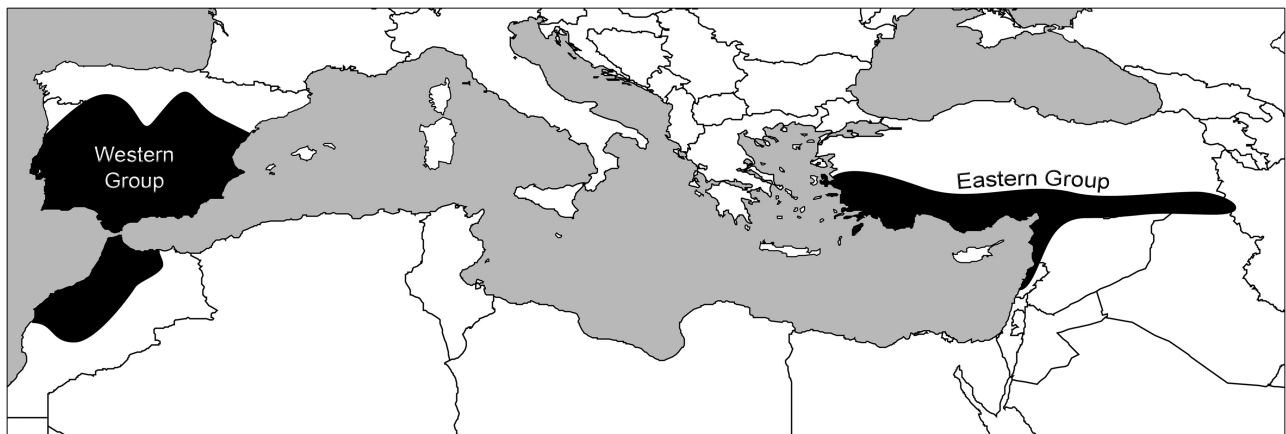

Figure 2. Current geographical distribution of the western and eastern clades of *Blanus*.

The main comparative analysis dealing with the cranial osteology of *Blanus* is the work of Gans & Montero (2008). These authors made a general description of the skull of *Blanus*, as part of a larger treatment of amphisbaenian skull morphology. In their analysis, the authors assumed that the skull of *Blanus* is morphologically primitive for amphisbaenians as a whole (as previously suggested by Kearney, 2003) and focused mainly on *B. cinereus* s.l., given that their analysis predates the distinction of the two Iberian lineages. Gervais (1853) also briefly described and figured the skull and lower jaw of *B. cinereus*. Kazi & Hipsley (2018) included four *Blanus* species in their geometric morphometric analysis of skull shape among Caribbean amphisbaenians and found that blanids differed significantly from their putative sister clade on Cuba, the Cadeidae. Other osteological remarks are scattered in the literature, mainly by palaeontologists when comparing fossils with extant taxa (e.g. Bolet *et al.*, 2014; Čerňanský *et al.*, 2015b, 2016). Nevertheless, Bedriaga (1884) already commented and illustrated the skulls of *B. cinereus* (s.l.) and *B. strauchi*, and a few skull characters were also mentioned by Boulenger (1885) and Zangerl (1944). Anatomical remarks and brief descriptions of the postcranial skeleton of *Blanus* were reported by other authors, such as Zangerl (1945), Renous *et al.* (1991) and Kearney (2002).

Here, we provide, for the first time, a detailed comparative analysis of the cranial osteology of all extant species of *Blanus* and discuss its implications for deciphering the phylogeny of the group (which is outside the scope of this paper) and our current understanding of the evolutionary history of this genus.

MATERIAL AND METHODS

Our analysis is based on five disarticulated skulls and 26 ethanol-preserved specimens that were studied by means of X-ray computed microtomography (μCT). The studied specimens include representatives of all extant species of *Blanus*. The disarticulated specimens are housed in the Department of Earth Sciences of the University of Turin (Massimo Delfino Herpetological Collection; MDHC), whereas the ethanol-preserved ones are stored in the collections of Museo Civico di Storia Naturale di Carmagnola (MCCI; Italy), Zoologische Staatssammlung München (ZSM; Germany) and Museum für Naturkunde Berlin (ZMB; Germany). A complete list of the studied specimens and the related measurements are given in the Supporting Information (Table S1).

Some of the specimens were analysed by μCT at the Multidisciplinary Laboratory of the 'Abdus Salam' International Centre of Theoretical Physics (ICTP; Trieste, Italy), using a system specifically designed for the study of archaeological and palaeontological

materials (Tuniz *et al.*, 2013). The μCT acquisitions were carried out using a sealed X-ray source (Hamamatsu L8121-03) at a voltage of 60/80 kV, a current of 120/140 μA and with a focal spot size of 5 μm. The X-ray beam was filtered by a 1 mm-thick aluminum absorber. A set of 1440 projections of the samples were recorded over a total scan angle of 360° by a flat panel detector (Hamamatsu C7942SK-25), with an exposure time/projection of 3–6 s. The resulting μCT slices were reconstructed in 32 bit TIFF format using the commercial DigiXCT software, obtaining an isotropic voxel size of ~8–11 μm (for detailed acquisition parameters, see the Supporting Information Table S2 and S3). Specimens digitized at the Museum für Naturkunde Berlin were scanned using a Phoenix nanotom X-ray tube at 80 kV and 120 μA, generating 1000 projections with 750 ms per scan. The cone beam reconstruction was performed using the datos|x-reconstruction software (GE Sensing & Inspection Technologies GmbH phoenix|x-ray datos|x v.2.0) and resulted in three-dimensional models with an effective voxel size of 4–8 μm. Later, the μCT data were segmented and three-dimensional models built with Avizo v.7.0 and Volume Graphics Studio Max v.2.2. Photographs of the isolated elements were taken at the University of Turin with a Leica M205 microscope equipped with the Leica application suite v.3.3.0.

Isolated bones are described following the order proposed by Evans (2008). The terminology used in the descriptions follows Evans (2008) and Gans & Montero (2008).

RESULTS

GENERAL SHAPE OF THE SKULL

The skull of *Blanus* (Figs 3–6) is elongated, slender and hourglass shaped in dorsal view, with a slight constriction at midlength. The posterior portion is moderately wider than the anterior one. In lateral view, the skull has a capsule-like shape and its dorsal outline is rather straight, because the anterior portion does not tilt distinctly in a ventral direction anteriorly to the frontoparietal suture (i.e. there is no craniofacial angle sensu Zangerl, 1944). Premaxillary and maxillary teeth are aligned at the same level (forming a weak arch in most cases); there is no step between them, unlike the step in *Bipes biporus* and *Trogonophis wiegmanni*, for example (see Gans & Montero, 2008).

NASAL

The nasals of *Blanus* are thin and subquadrangular paired bones (Fig. 7A, B), with roughly straight lateral
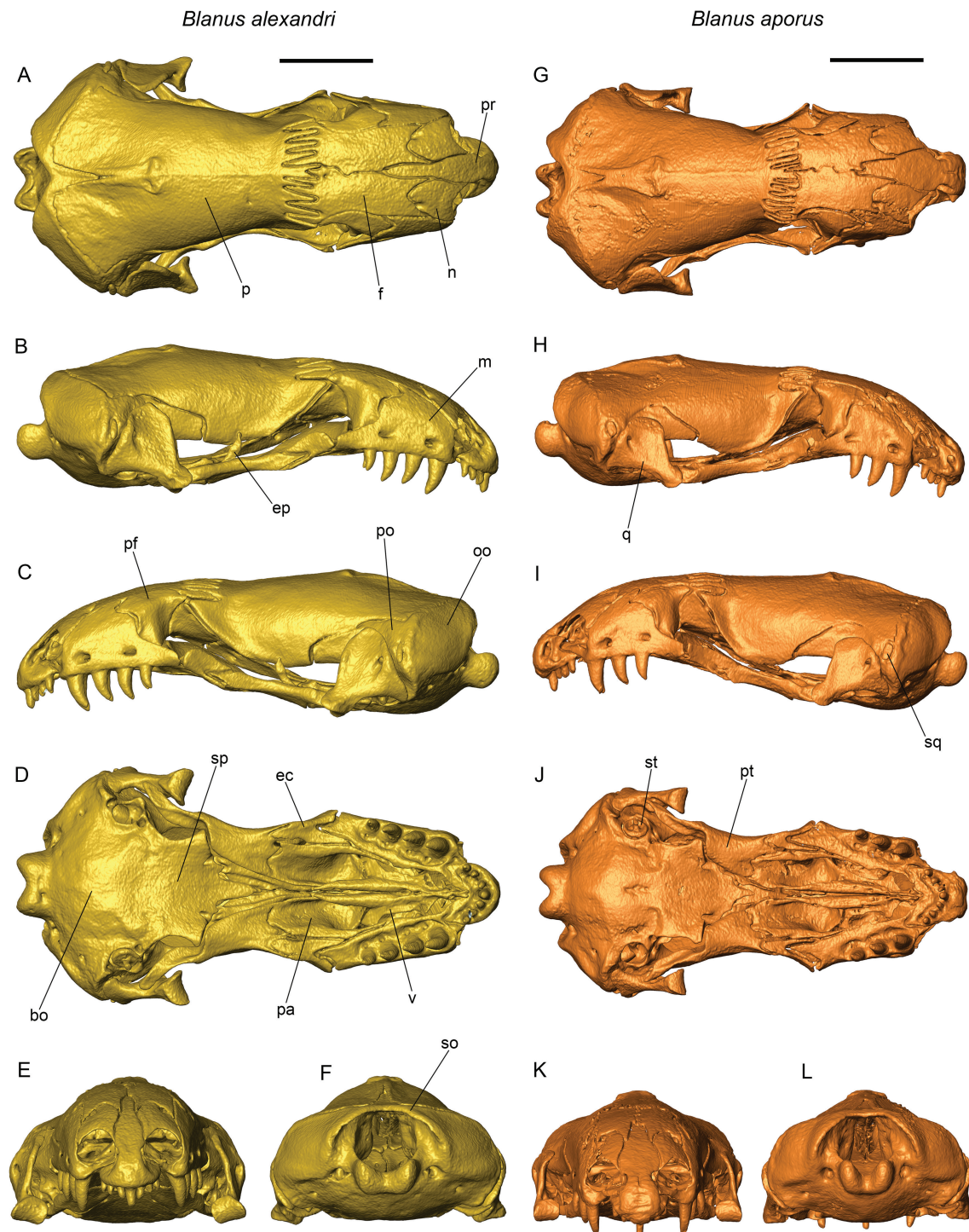
Figure 3. A–F, articulated skull of *Blanus alexandri* (MCCI R-1634) in dorsal (A), right lateral (B), left lateral (C), ventral (D), anterior (E) and posterior (F) views. G–L, articulated skull of *Blanus aporus* (ZMB 14116) in dorsal (G), right lateral (H), left lateral (I), ventral (J), anterior (K) and posterior (L) views. Abbreviations: bo, basioccipital; ec, ectopterygoid; ep, epipterygoid; f, frontal; m, maxilla; n, nasal; oo, otooccipital; p, parietal; pa, palatine; pf, prefrontal; po, prootic; pr, premaxilla; pt, pterygoid; q, quadrate; so, supraoccipital; sp, sphenoid; sq, squamosal; st, stapes; v, vomer. Scale bars: 2 mm.
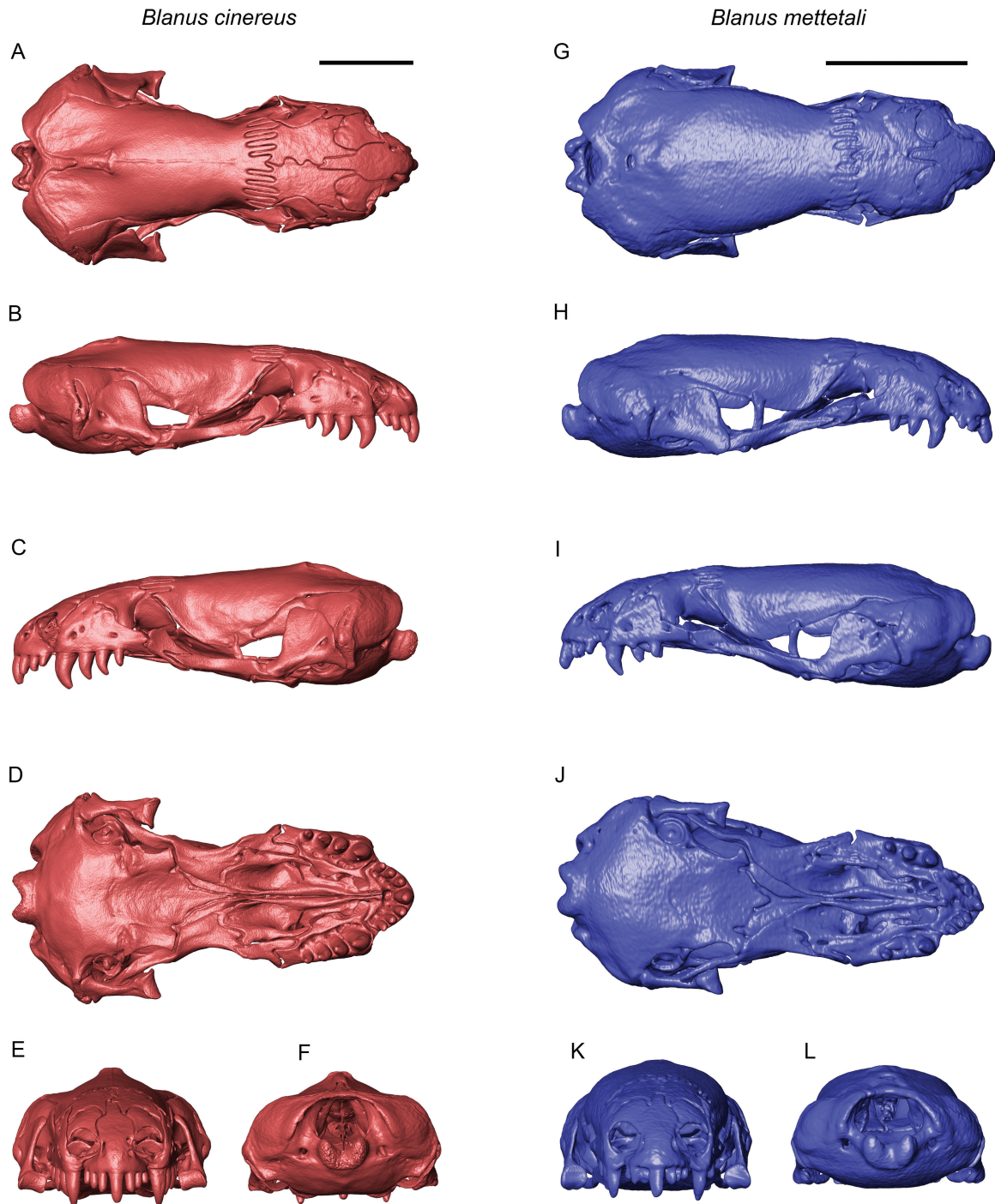
Figure 4. A–F, articulated skull of *Blanus cinereus* (ZSM 27-1988-1) in dorsal (A), right lateral (B), left lateral (C), ventral (D), anterior (E) and posterior (F) views. G–L, articulated skull of *Blanus mettetali* (MCCI R-1182) in dorsal (G), right lateral (H), left lateral (I), ventral (J), anterior (K) and posterior (L) views. Scale bars: 2 mm.
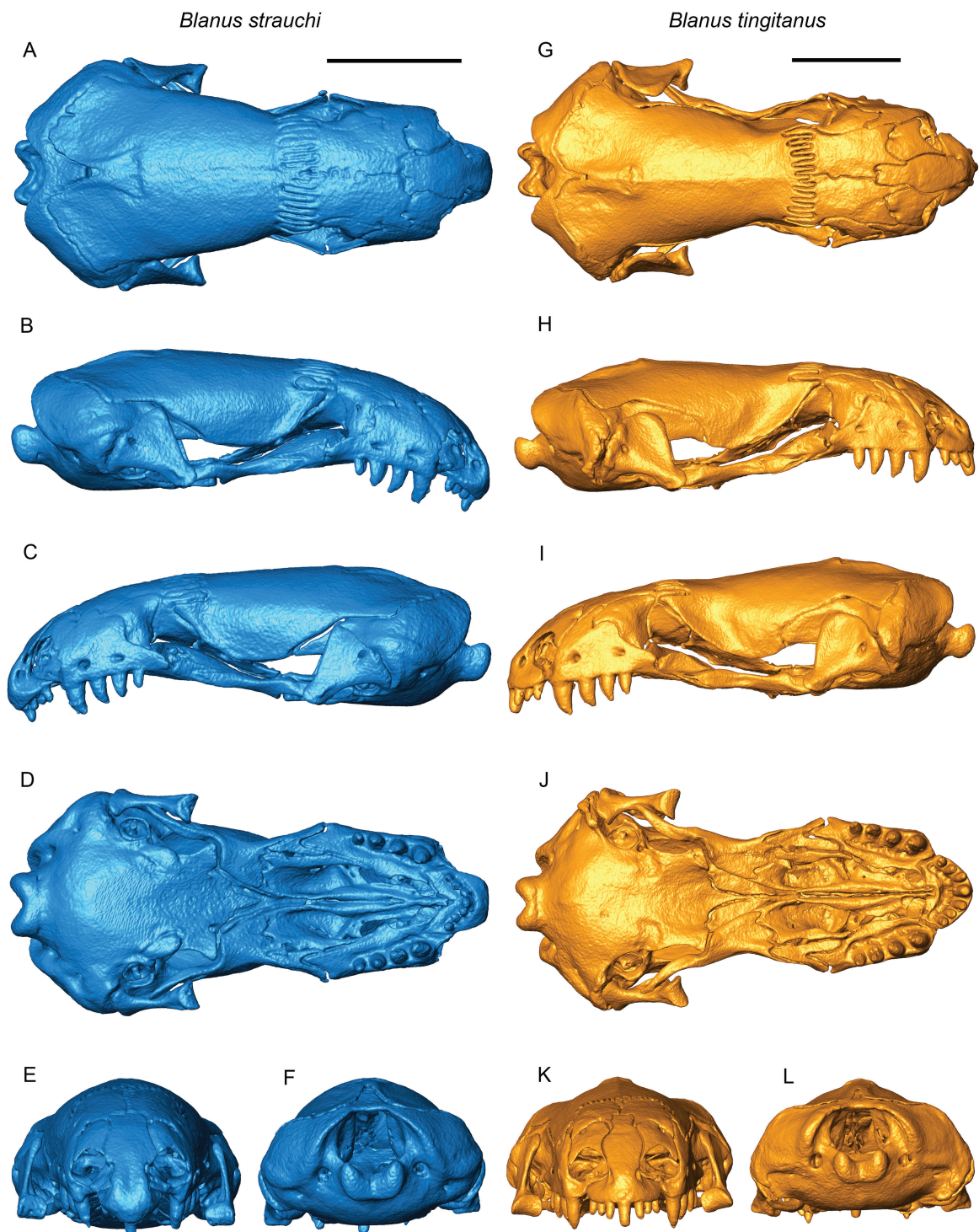
Figure 5. A–F, articulated skull of *Blanus strauchi* (MCCI R-1668) in dorsal (A), right lateral (B), left lateral (C), ventral (D), anterior (E) and posterior (F) views. G–L, articulated skull of *Blanus tingitanus* (MCCI R-1176) in dorsal (G), right lateral (H), left lateral (I), ventral (J), anterior (K) and posterior (L) views. Scale bars: 2 mm.
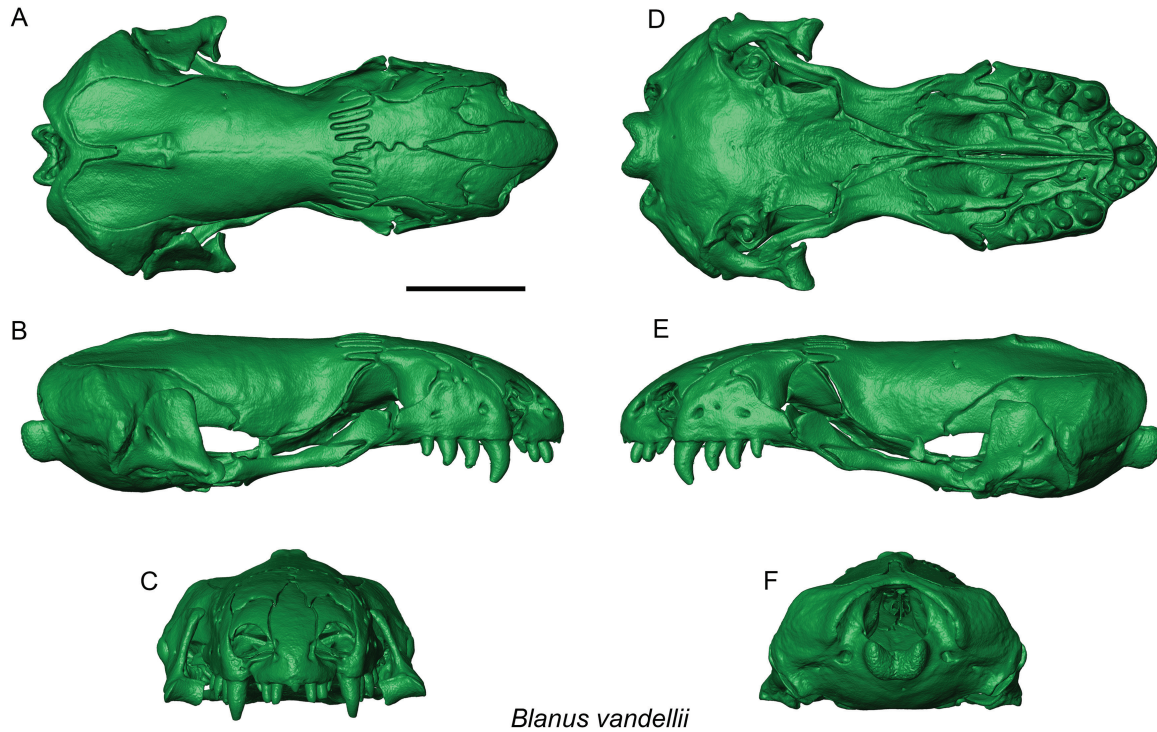
Figure 6. Articulated skull of *Blanus vandellii* (ZSM 227-1975) in dorsal (A), right lateral (B), anterior (C), ventral (D), left lateral (E) and posterior (F) views. Scale bars: 2 mm.

and medial margins, a strongly concave anterior margin and a convex posterior margin. They are concave in the ventral direction. At the corners of the anterior margin there are the anteromedial and the anterolateral processes, both pointed. The former is roughly two or three times longer than the latter. The wide and posteriorly rounded posterior process contacts the concave anterior margin of the corresponding frontal. Both the ventral and the dorsal surfaces of the nasal are smooth, but the articular surface with the ascending nasal process of the premaxilla is visible in dorsal view along the entire medial margin (Fig. 7A). Another articular surface, that with the facial process of the maxilla, is present along the lateral margin.

FRONTAL

The frontals are short and rectangular paired bones (Fig. 7C–E), with subparallel lateral and medial margins. The former is very slightly concave, whereas the latter bears the wavy interfrontal suture. The anterior end is as wide as the posterior end. Both an anteromedial and an anterolateral process are present at the anterior corners of the bone; they are moderately developed, defining a distinctly concave anterior margin. The articular surface with the facial process of the maxilla is visible on the lateral side of the

anterolateral process, whereas the articular surface with the ascending nasal process of the premaxilla covers the medial side of the anteromedial process. No clearly developed posterolateral process is present. The dorsal surface is smooth and almost flat, with only a weak ventral bending of the anterolateral process. On the ventral surface, the laminar crista cranii is well developed (Fig. 7D). This structure runs from the midpoint of the medial margin to the posterolateral corner of the bone, originating a posteromedially concave, ventrally directed and wide ventral process. The rounded posteroventral margin of this process contacts the tabulosphenoid. Its anterolateral surface is split into two portions by a ridge-like anterior process, which contacts the palatine ventrally. The anterior portion of this surface is smooth, whereas the posterior one shows the articular surface with the dorsal process of the prefrontal by the anterodorsal corner and that with the anterolateral process of the parietal at the posterodorsal corner (Fig. 7E). The posterior margin of each frontal is strongly interdigitated and carries five (sometimes four in *B. aporus* and *B. vandellii*) long and slender digits. In *B. aporus* and *B. strauchi*, six (*B. strauchi* MDHC 286 and 288, the left frontal of *B. aporus* ZSM 173-1975 and the right frontals of *B. aporus* MCCI R-1680 and *B. strauchi* MDHC 287) or even seven (the right frontals of *B. strauchi* MDHC 288
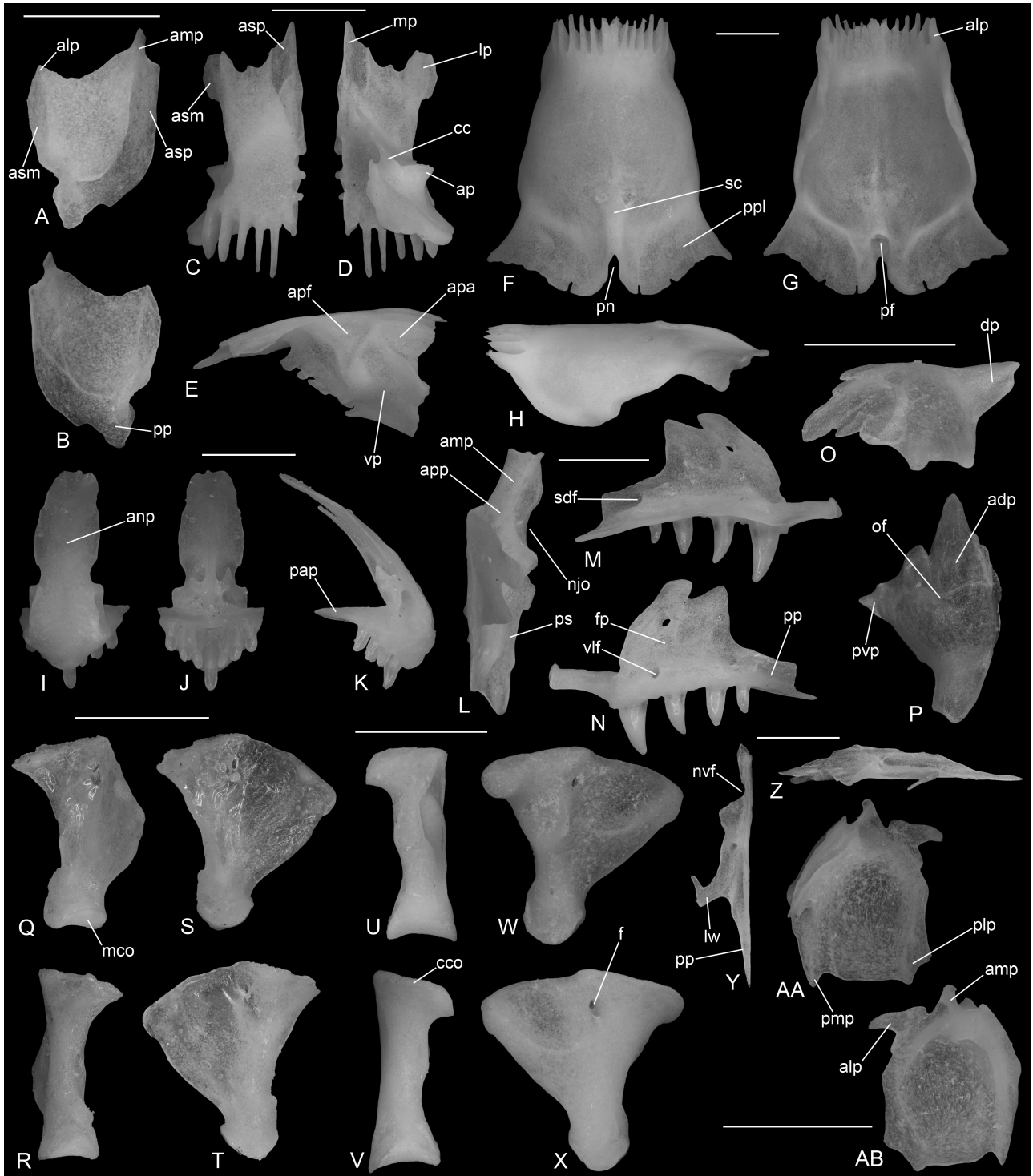
Figure 7. A–B, *Blanus strauchi* (MDHC 288), left nasal in dorsal (A) and ventral (B) views. C–E, *B. strauchi* (MDHC 286), left frontal in dorsal (C), ventral (D) and lateral (E) views. F–H, *B. strauchi* (MDHC 286), parietal in dorsal (F), ventral (G) and left lateral (H) views. I–K, *B. strauchi* (MDHC 287), premaxilla in anterior (I), posterior (J) and right lateral (K) views. L–N, *B. strauchi* (MDHC 287), left maxilla in dorsal (L), medial (M) and lateral (N) views. O–P, *B. strauchi* (MDHC 287), left prefrontal in lateral (O) and dorsal (P) views. Q–T, *Blanus vandellii* (MDHC 156), left quadrate in anterior (Q), posterior (R), medial (S) and lateral (T) views. U–X, *B. strauchi* (MDHC 287), left quadrate in anterior (U), posterior (V), medial (W) and lateral (X) views. Y–Z, *B. strauchi* (MDHC 288), left vomer in dorsal (Y) and lateral (Z) views. AA–AB, *B. strauchi* (MDHC

and *B. aporus* ZSM 173-1975) digits are sometimes recognizable, because some of them appear to be split into two.

PARIETAL

The parietal is unpaired and strongly elongated anteroposteriorly (Fig. 7F–H). In dorsal view, the posterior portion is wider than the anterior one, with the more constricted part placed close to the anterior end. The lateral margins of the bone bend strongly in the ventral direction, covering laterally the anterior portion of the braincase. As a result, the parietal appears strongly concave ventrally and takes a dorsally rounded vaulted shape. Very deep and narrow interdigitations are present on the anterior margin; usually, eight digits are present, except for *B. aporus*, *B. strauchi* and *B. vandellii*, in which the number of digits can be also six (*B. aporus* ZSM 2129-2009), seven (*B. aporus* ZMB 14116, *B. aporus* ZSM 2128-2009, *B. aporus* ZSM 37-1993-1, *B. aporus* ZSM 381-1976, *B. vandellii* ZSM 652-0-2 and *B. vandellii* ZSM 653-0-2), nine (*B. strauchi* MCCI R-1635, *B. strauchi* MDHC 287, *B. aporus* ZSM 173-1975 and *B. aporus* ZSM 264-1988-1), ten (*B. aporus* MCCI R-1680) or 11 (*B. strauchi* MDHC 286 and 288). Moderately wide and pointed anterolateral processes are recognizable by the anterolateral corners, flanking the interdigitations and not projecting beyond them. A couple of large posterior plates develop posteriorly from the posterior margin. The plates cover the supraoccipital dorsally and are separated by a long and narrow or moderately wide parietal notch. The supraoccipital crest of the supraoccipital fits within this notch. Anterior to the notch, a sagittal crest runs briefly on the dorsal surface, ending with a moderately developed dorsal knob. The crest is rather narrow and sharp in most specimens of *B. cinereus* and *B. vandellii* (even if some variation may occur: e.g. *B. vandellii* ZSM 652-0-1 and 227-1975), whereas it is wider and more rounded in the other species. Only in *B. mettetali* (Fig. 4G) and in two specimens of *B. vandellii* (ZSM 175-1993-1 and 175-1993-2), the crest appears not to be present. These two specimens of *B. vandellii* also show a very wide and U-shaped parietal notch, although this feature

and the absence of the supraoccipital crest might be attributable to a juvenile condition, also implied by a lower degree of fusion of the braincase. The dorsal knob does not reach the parietal midlength. In ventral view, the notch is preceded by a very small but moderately deep parietal fossa (Fig. 7G). Both the dorsal and the ventral surface of the parietal are smooth. However, on the ventral surface, two shallow concave areas are visible near the anterior margin, and two low and transverse ridges mark the bases of the posterior plates. There is no parietal foramen.

PREMAXILLA

The unpaired premaxilla (Figs 7I–K, 8) has a long and wide ascending nasal process, possessing slightly convex lateral margins and a smooth anterior surface. The process narrows towards the truncated or pointed dorsal end. In a single specimen of *B. strauchi* (MDHC 286), the nasal process is arrow shaped in anterior view. In some specimens of the eastern species (e.g. *B. aporus* ZSM 173-1975), a narrow dorsoventral depression is present in the middle of the anterodorsal surface of the bone. When present, this depression has a highly variable depth, varying from very deep in *B. aporus* ZSM 173-1975 to barely recognizable in *B. alexandri* MCCI R-1633, whereas *B. aporus* ZSM 37-1993-1 would present an intermediate condition. The alveolar portion of the bone bears seven (or five in ZSM 37-1993-1 and 381-1976, six in ZSM 37-1993-2, eight in ZMB 14116; all of these specimens belonging to *B. aporus*) pleurodont, cylindrical and monocuspid teeth, among which the central one is the largest. As a general trend, premaxillary teeth of the species of the Eastern Group are smaller relative to those of the maxilla if compared with those of the species of the Western Group (compare e.g. Fig. 3B, C, H, I with Fig. 4B, C). A certain degree of variation seems to occur, however, with teeth of some western specimens that approach the smaller condition usually seen in eastern ones (as in *B. vandellii* ZSM 227-1975; Fig. 6B, E). Dorsally to the teeth, the palatal processes extends posteriorly. These processes are separated from one another by a small U-shaped notch. At the junction of the nasal process with the alveolar plate, a very wide

287), right septomaxilla in dorsal (AA) and ventral (AB) views. Abbreviations: adp, anterodorsal process; alp, anterolateral process; amp, anteromedial process; anp, ascending nasal process; ap, anterior process; apa, articular surface with the parietal; apf, articular surface with the prefrontal; app, anterior premaxillary process; asm, articular surface with the maxilla; asp, articular surface with the premaxilla; cc, crista cranii; cco, cephalic condyle; dp, dorsal process; f, foramen; fp, facial process; lp, lateral process; lw, lateral wing; mco, mandibular condyle; mp, medial process; njo, notch of the foramen for Jacobson's organ; nvf, notch of the vomeronasal fenestra; of, orbitonasal flange; pap, palatal process; pf, parietal fossa; plp, posterolateral process; pmp, posteromedial process; pn, parietal notch; pp, posterior process; ppl, posterior plates; ps, palatal shelf; pvp, posteroventral process; sc, sagittal crest; sdf, superior dental foramen; vlf, ventrolateral foramen; vp, ventral process. Scale bars: 1 mm.

foramen of the longitudinal canal opens anterolaterally on each side of the nasal process. A second foramen can be seen clearly, at least in *B. aporus* (all specimens, except for ZSM 2129-2009), *B. vandellii* (all specimens, except for ZSM 175-1993-2; see also Bolet *et al.*, 2014), *B. cinereus* (both specimens) and *B. strauchi* (MCCI R-1668). In *B. aporus* and in one specimen of *B. vandellii* (ZSM 653-0-2), this second foramen may lack the lateral wall, giving a concave appearance to the base of the process in anterior view. Another wide foramen is visible on the posterior surface, by each side of the distinctly developed septonasal crest (Fig. 7J). In lateral view, the anterior outline of the premaxilla is flat and not overhanging beyond the central tooth position in *B. cinereus* (Fig. 8C), *B. mettetali* (Fig. 8D), *B. tingitanus* (Fig. 8F) and *B. vandellii* (Fig. 8G), but overhangs anteriorly in *B. alexandri* (Fig. 8A), *B. aporus* (Fig. 8B) and *B. strauchi* (Fig. 8E). In ventral view, the same outline is rounded in *B. cinereus* (Fig. 4D), *B. mettetali* (Fig. 4J), *B. tingitanus* (Fig. 5J) and *B. vandellii* (Fig. 6D). *Blanus aporus* (Fig. 3J) and *B. strauchi* (Fig. 5D), in contrast, display a variable morphology, with the anterior outline that varies from distinctly squared to more roundish. Lastly, the outline is intermediate between the squared and the rounded condition in the two specimens of *B. alexandri* included in our analysis (Fig. 3D).

Maxilla

Blanus has short maxillae (Fig. 7L–N) bearing a well-developed palatal shelf, which narrows posteriorly in dorsal view. On the anterior half of the medial margin of the shelf, there is a wide and deep notch, marking the lateral margin of the foramen for Jacobson's organ (Fig. 7L). Posteriorly to this notch, an oblique groove is visible on the dorsal surface of the shelf. The anterior premaxillary process shows a very well-developed, wide and squared anteromedial process by the medial corner (Fig. 7L), whereas the anterolateral process is completely lacking. The anteromedial process is ventrally concave and overlaps the corresponding palatal process of the premaxilla. The posterior process is very short and pointed. A very distinct and high step is present on its dorsal margin (Fig. 7N). The wide facial process is subtriangular in lateral view; its anterior margin is slightly convex, whereas the posterior one is concave and wavy. A moderately long (less developed in *B. alexandri*; Fig. 3B, C), slender and pointed projection develops posterodorsally from the dorsal end of the process; a second very short (more developed in *B. aporus*, Fig. 3H, I, and *B. strauchi*, Fig. 5B, C), moderately wide and rounded projection is present on the posterior margin, ventral to the former. The base of the facial process is pierced anteroposteriorly by the superior alveolar canal, whose anterior and posterior openings are located on the medial surface of the process. The anterior opening, the vomeronasal foramen, is small and located posteriorly to the anterior margin of the process, whereas the posterior one, the superior dental foramen, is very wide and situated near the step on the posterior process. Two (three in *B. aporus* ZSM 264-1988-1 and *B. cinereus* ZSM 27-1988-2, the left maxilla of *B. vandellii* ZSM 652-0-1 and *B. cinereus* ZSM 27-1988-1 and the right maxilla of *B. aporus* ZSM 2128-2009, *B. vandellii* ZSM 548-2003 and *B. vandellii* ZSM 653-0-1) wide ventrolateral foramina represent
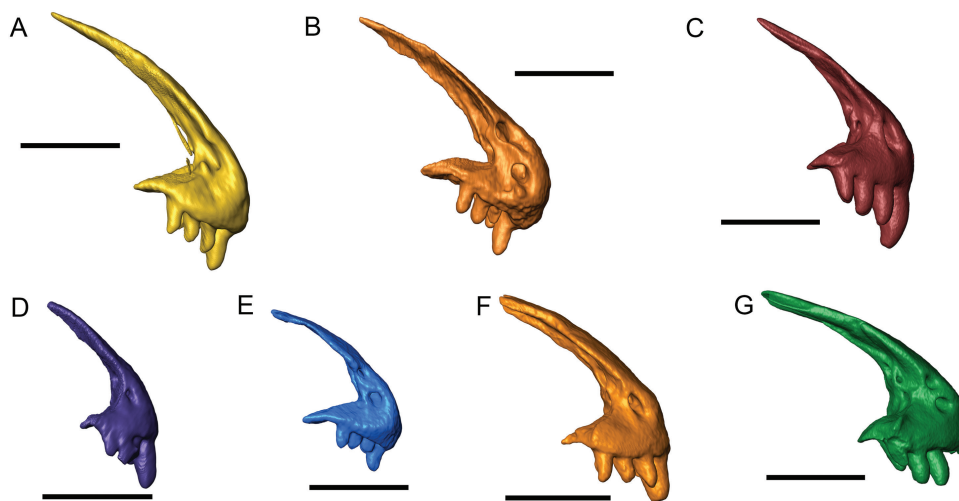

Figure 8. Premaxillae of *Blanus alexandri* (MCCI R-1634; A), *Blanus aporus* (ZMB 14116; B), *Blanus cinereus* (ZSM 27-1988-1; C), *Blanus mettetali* (MCCI R-1182; D), *Blanus strauchi* (MCCI R-1668; E), *Blanus tingitanus* (MCCI R-1176; F) and *Blanus vandellii* (ZSM 227-1975; G) in right lateral view. Scale bars: 1 mm.

the lateral openings of the canal. The lateral surface of the bone is smooth. The alveolar border of the maxilla bears subpleurodont, robust and canine-like teeth, the crowns of which bend posteromedially. The number of teeth can be three or four, and their size decreases posteriorly. However, Bailon (1991) mentioned maxillae of *B. cinereus* (s.l., given that the two Iberian clades were still unknown at the time) bearing five teeth, the anteriormost of which being less developed, and a similar condition is observed in the left maxilla of ZSM 37-1993-2 (*B. aporus*). The only known maxillae of the extinct *B. mendezi* also have five maxillary teeth (Bolet *et al.*, 2014). The teeth are not present at the level of the posterior process.

PREFRONTAL

The prefrontal of *Blanus* (Fig. 7O, P) has a small and anteromedially concave body, the orbitonasal flange, whose external surface is smooth. From the dorsal margin of the flange, a short and laminar anterodorsal process develops anteriorly. The dorsal surface of this process is divided into two halves by a low transverse ridge. The anterior half is the articular surface with the facial process of the maxilla. By the ventrolateral corner of the orbitonasal flange, there is a very short and roughly squared posteroventral process. A shallow but wide notch marking the medial margin of the lacrimal foramen is present on the lateral margin, dorsal to the latter process. The posterodorsally developed dorsal process is located at the posterodorsal corner of the flange; it is very short, triangular and has a truncated or pointed distal end. There is no palpebral crest.

SQUAMOSAL

Owing to its varying position relative to the quadrate in different species and to its presence in taxa distantly related, there is a degree of uncertainty on the real homology of the so-called squamosal in amphisbaenians and the corresponding bone in lacertilians (Gans & Montero, 2008). However, here

we follow Gans & Montero (2008) in naming this bone as such.

The squamosal seems to be absent in *B. tingitanus* (Fig. 5H, I) and present in the other species. Nevertheless, it has to be taken into account that its purported absence in the former species might simply reflect our inability to detect it in the single specimen available for study. Moreover, it is worth noting that Gans & Montero (2008) mentioned the absence of this bone in *B. aporus*, in contrast to our own results. This very small bone is slender and either elongated (Fig. 4B, C) or subelliptical (e.g. Fig. 3H, I).

QUADRATE

The quadrates (Figs 7Q–X, 9) have a roughly triangular shape in lateral view. The body of the bone is a posteriorly concave pillar structure, with a cephalic condyle on its dorsal end and a mandibular condyle on the ventral one. The former is anteroposteriorly elongated and slender in dorsal view, whereas the latter is mediolaterally expanded and composed of two very poorly developed portions that are similar in size. A well-developed and wing-like osseous lamina projects anteriorly from the lateral surface of the pillar, bending medially to follow the lateral wall of the braincase. The conch is therefore not present. In *B. aporus* and *B. strauchi*, a distinct and rather robust ridge is present on the posteromedial side of the pillar (Fig. 9B). This ridge is lower and thinner in *B. alexandri*, *B. cinereus* and *B. tingitanus* (Fig. 9A) and poorly developed or not clearly recognizable in *B. mettetali* and *B. vandellii* (Fig. 9C). A wide foramen pierces the anterolateral lamina near the cephalic condyle.

EPIPTERYGOID

The epipterygoid is usually not present in amphisbaenians, but it is retained at least in some individuals of *Blanus* (Gans & Montero, 2008). It appears to be absent in the single studied specimen
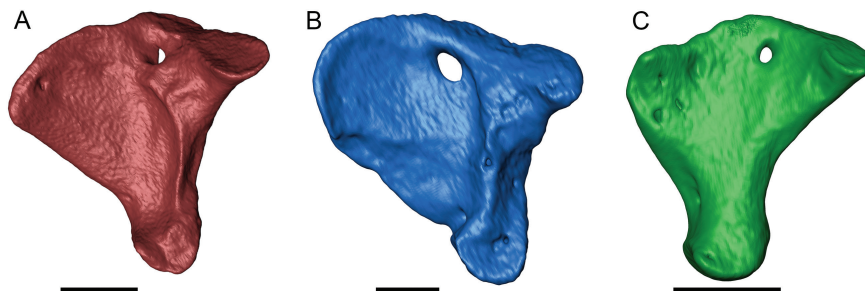

Figure 9. Right quadrate of *Blanus cinereus* (ZSM 27-1988-1; A), *Blanus strauchi* (MCCI R-1635; B) and *Blanus vandellii* (ZSM 175-1993-1; C) in medial view. Scale bars: 0.5 mm.

of *B. tingitanus* (Fig. 5G–L) and can be either present or absent in *B. aporus*, *B. alexandri* and *B. strauchi*. It is present in *B. cinereus*, *B. mettetali* and *B. vandellii*. When present, this rod-like bone is distinctly curved, with a posterior concavity, and mediolaterally compressed (e.g. Fig. 3B, C). Only in ZMB 14116 (*B. aporus*), its morphology is distinctly different from that of the other epipterygoids (i.e. roughly triangular and not rod-like). According to Gans & Montero (2008), *B. aporus* and *B. strauchi* should lack this bone, but we have been able to detect it in at least some of the studied specimens.

VOMER

The paired vomers are very slender, thin and strongly elongated anteroposteriorly (Fig. 7Y, Z). Their laminar body is poorly concave in the dorsal direction and presents a well-developed lateral wing roughly at midlength. The lateral wing is slender, finger-like and presents an anteriorly directed concavity (Fig. 7Y). Anterior to the wing, the lateral margin of the bone shows two wide notches, the anteriormost and deepest of which is the medial margin of the vomeronasal fenestra. Posterior to the wing, the vomer shows a very long, slender and pointed posterior process. The dorsal surface of this process is covered by the articular surface with the vomerine process of the palatine, the lateral margin of which is marked by a low ridge by the base of the lateral wing. The anterior end of the vomer is also narrow. A well-developed ridge runs along the entire medial margin of the bone, projecting dorsally and lowering posteriorly. In lateral view, the anterior end of this ridge is forked, showing two short and slender processes flanking a deep notch (Fig. 7Z). Roughly at one-third of the length of the bone, the ridge is connected to the laminar body of the vomer by a moderately stocky osseous expansion, anteroposteriorly pierced by a foramen. The ventral surface of the vomer is smooth.

SEPTOMAXILLA

Blanus has small, thin, ventrally concave and subquadrangular septomaxillae (Fig. 7 AA, AB). This bone shows four short processes, situated at its four corners. A very small anteromedial process and a small posteromedial one are present by the two ends of the medial margin, whereas the anterolateral and the posterolateral processes are located by the ends of the lateral margin. Both lateral processes are wider than the medial ones. The anterior processes are directed anteriorly; the posteromedial one is directed posteriorly, and the posterolateral one develops in a posterolateral direction, slightly bending dorsally. A ventrally directed osseous expansion is present by

the anteromedial corner, continuing posteriorly in a ridge running along the medial margin and laterally with a very low and arched ridge that borders laterally the ventral surface (Fig. 7AB). A moderately developed ridge, anteroposteriorly pierced by a canal, is present along the medial margin on the dorsal surface.

PALATINE

The palatines are anteroposteriorly elongated and blade-like bones (Fig. 10A, B), with straight and posteriorly convergent lateral and medial margins. These bones are strongly concave ventrally, because of the presence of a very deep and wide choanal duct along the ventral surface. The anterior half of the medial margin bends very slightly in a lateral direction, covering a small part of the duct. The dorsal surface is smooth. Long, pointed and slender vomerine and maxillary processes develop in the anterior direction from the anteromedial and the anterolateral corners of the bone, respectively; the vomerine process is slightly longer than the maxillary one. A well-developed palatine ridge runs on the dorsal surface of the bone along the anterior margin, lowering towards its medial side. This ridge projects beyond the lateral margin of the palatine, originating a small and triangular lateral expansion. There is no infraorbital foramen. The pterygoid process is very long and wide and has a pointed posterior end. The articular surface with the palatine process of the pterygoid is recognizable on the ventral surface of this process. In the middle of the lateral margin of the bone, a small and thumb-like laminar expansion is present, projecting posterolaterally and contacting a similar structure on the pterygoid. The expansion appears to be slightly more developed in *B. aporus* and *B. tingitanus* than in other species.

PTERYGOID

The anterior half of the pterygoid (Fig. 10C, D) is dorsally concave and made up by a small, pointed and laminar palatine process and by a long and pointed pterygoid flange. These two processes are separated by a very shallow pterygoid recess. The large and triangular articular surface with the pterygoid process of the palatine is visible on the dorsal surface of the palatine process. Dorsally, a well-developed ridge for the insertion of the superficial pseudotemporal muscle runs along the entire lateral margin of the pterygoid flange. On its ventral surface, in contrast, only a small hint of a ridge is recognizable by the anterior tip. The articular surfaces with the posterodorsal and the posteroventral processes of the ectopterygoid are present on the dorsal and the ventral surfaces of the flange, respectively. The articular surface with the
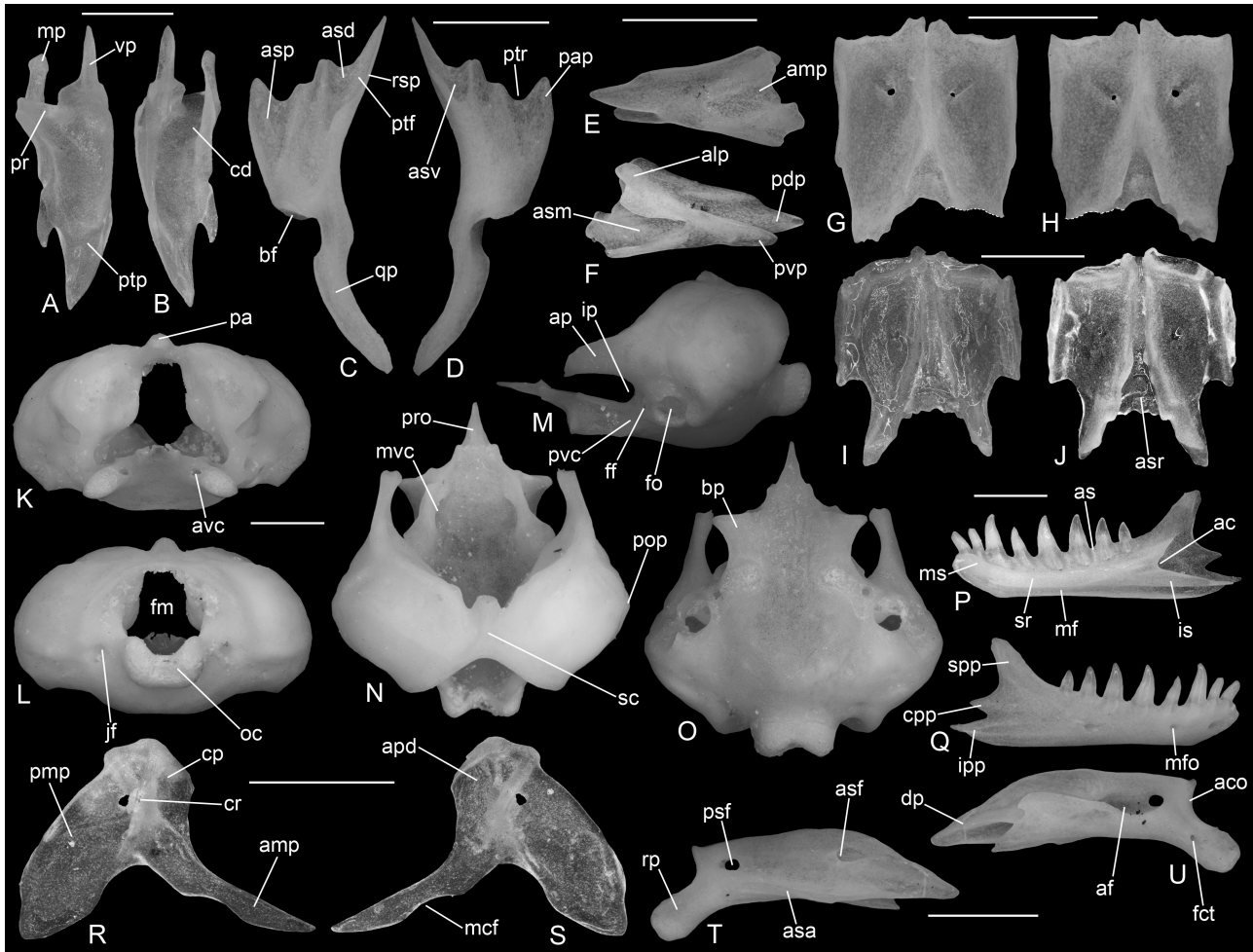
Figure 10. A–B, *Blanus strauchi* (MDHC 287), left palatine in dorsal (A) and ventral (B) views. C–D, *B. strauchi* (MDHC 287), right pterygoid in dorsal (C) and ventral (D) views. E–F, *B. strauchi* (MDHC 288), left ectopterygoid in medial (E) and lateral (F) views. G–H, *Blanus vandellii* (MDHC 156), tabulosphenoid in dorsal (G) and ventral (H) views (the left posterior process is broken). I–J, *B. strauchi* (MDHC 287), tabulosphenoid in dorsal (I) and ventral (J) views. K–O, *B. strauchi* (MDHC 287), otooccipital region in anterior (K), posterior (L), left lateral (M), dorsal (N) and ventral (O) views. P–Q, *B. strauchi* (MDHC 287), right dentary in medial (P) and lateral (Q) views. R–S, *B. strauchi* (MDHC 287), left coronoid in medial (R) and lateral (S) views. T–U, *B. vandellii* (MDHC 156), right compound bone in lateral (T) and medial (U) views. Abbreviations: ac, alveolar canal; aco, articular condyle; af, adductor fossa; alp, anterolateral process; amp, anteromedial process; ap, alar process; apd, articular surface with the superior posterior process of the dentary; as, alveolar shelf; asa, articular surface with the angular; asd, articular surface with the posterodorsal process of the ectopterygoid; asf, anterior surangular foramen; asm, articular surface with the maxilla; asp, articular surface with the palatine; asr, articular surface with the parasphenoid rostrum of the sphenoid; asv, articular surface with the posteroventral process of the ectopterygoid; avc, anterior opening of the Vidian canal; bf, basipterygoid fossa; bp, basipterygoid process; cd, choanal duct; cp, coronoid process; cpp, central posterior process; cr, coronoid ridge; dp, dentary process; fct, foramen for the chorda tympani; ff, facial foramen; fm, foramen magnum; fo, fenestra ovalis; ip, incisura prootica; ipp, inferior posterior process; is, intramandibular septum; jf, jugular foramen (concavity of the vagus foramen); mcf, notch of the mandibular central foramen; mf, Meckelian fossa; mfo, mental foramen; mp, maxillary process; ms, mandibular symphysis; mvc, medial opening of the Vidian canal; oc, occipital condyle; pa, processus ascendens; pap, palatine process; pdp, posterodorsal process; pmp, posteromedial process; pop, paroccipital process; pr, palatine ridge; pro, parasphenoid rostrum; psf, posterior surangular foramen; ptf, pterygoid flange; ptp, pterygoid process; ptr, pterygoid recess; pvc, posterolateral opening of the Vidian canal; pvp, posteroventral process; qp, quadrate process; rp, retroarticular process; rsp, ridge for the insertion of the superficial pseudotemporal muscle; sc, supraoccipital crest; spp, superior posterior process; sr, subdental ridge; vp, vomerine process. Scale bars: 1 mm.

posteroventral process is small and limited to the anterior tip, whereas the one with the posterodorsal process is longer. A small and anteriorly directed expansion, contacting the lateral expansion of the palatine, is present on the medial margin of the pterygoid flange. There are no pterygoid teeth on the ventral surface. The quadrate process is slender, moderately long and slightly sigmoid in dorsal view, with a lateral concavity; its posterior end is flat and can be either rounded or pointed in different individuals of the same species. Its joint with the anterior portion of the pterygoid is mediolaterally enlarged. The fossa columellae is rather shallow. The basipterygoid fossa is very wide, flat and posteromedially directed. It continues posteriorly in a wide and distinctly concave surface for the insertion of the pterygoideus muscle.

ECTOPTERYGOID

The ectopterygoids are small and subtriangular (Fig. 10E, F). The anterior end of these bones is represented by a moderately wide and anteriorly truncated anteromedial process, whose ventrolateral surface is completely covered by the articular surface with the posterior process of the maxilla. The anterior margin of this process is truncated and shows a small notch in the middle. The posterior end of the ectopterygoid is forked, because of the presence of two processes: a rounded posteroventral and a pointed posterodorsal process. The former is smaller and shorter than the latter. The pterygoid flange of the pterygoid is lodged between these two processes. A moderately wide and lappet-like anterolateral process develops anterodorsally from the middle of the dorsal margin of the bone. The dorsal margin of the posteroventral process and the ventral margin of the anterolateral process define a low ridge that runs on the lateral surface of the bone. The medial surface of the ectopterygoid is smooth and medially concave.

TABULOSPHENOID

The tabulosphenoid is an unpaired, laminar and quadrangular bone (Fig. 10G–J). It is dorsally concave, very slightly longer than it is wide, and has subparallel and straight lateral margins. The anterior margin is also straight, except for a small expansion in the middle. The posterior margin, in contrast, shows two moderately wide and long posterior processes flanking a deep and U-shaped notch. This notch continues in a V-shaped articular surface on the ventral surface of the bone (Fig. 10H, J). This V-shaped surface, which lodges the parasphenoid rostrum of the sphenoid, is bordered laterally by two robust ridges, which continue anteriorly in low ridges running along the midline towards the anterior margin. The latter ridges usually

remain well separated, but they can fuse medially (at least in *B. vandellii*, MDHC 156; Fig. 10H). A small foramen pierces the tabulosphenoid by both sides of these low ridges, near midlength. The dorsal surface of the bone is smooth, except for a moderate swelling by the V-shaped ventral surface. In contrast to all the other specimens studied, *B. vandellii* ZSM 175-1993-2, *B. aporus* ZSM 2129-2009, *B. aporus* ZSM 264-1988-1, *B. cinereus* ZSM 27-1988-2 and *B. aporus* ZSM 381-1976 show a split tabulosphenoid, divided longitudinally into two halves.

GENERAL FEATURES OF THE OTOOCCIPITAL REGION

Nine bones compose the otooccipital region of *Blanus* (Fig. 10K–O), namely the basioccipital, the sphenoid, the two elements-X, the two prootics, the supraoccipital and the two otooccipitals. These bones are fused in adults, but separate in juveniles. There is strong variation in the fusion of the elements-X, in particular (Gans & Montero, 2008). The region is distinctly compressed dorsoventrally. The foramen magnum is wide and subcircular, and the occipital condyle is also wide (Fig. 10L). The latter is composed by the basioccipital and both the otooccipitals, but the suture between them is not visible and therefore it is impossible to define how much they contribute to its formation (Jollie, 1960). In dorsal view, the condyle presents a deep notch in the middle, whereas in posterior view it is strongly U-shaped. The very wide and circular fenestra ovalis is the only visible opening on the lateral side of the braincase (Fig. 10M), because the occipital recess is lacking in amphisbaenians (Jollie, 1960). The fenestra completely occupies the anterior inferior process of the prootic and is defined by the sphenoid anteroventrally, by the basioccipital posteroventrally, by the prootic anterodorsally and by the otooccipital posterodorsally. The fenestra does not open directly in the cochlear cavity, but in a concave area connected posteriorly with the latter. The semicircular canals are very poorly distinguishable, but the otic capsule is strongly enlarged, forming an ellipsoidal bulge.

BASIOCCIPITAL

The unpaired basioccipital is subhexagonal, roughly as long as it is wide and dorsally concave (Fig. 10L, O). Both the dorsal and ventral surfaces are smooth, but there is a shallow concave area in the middle of the anterior half of the latter, continuing anteriorly on the sphenoid. The lateral wings of the bone are poorly developed, and no sphenooccipital tubercle is present. In dorsal view, the anterior margin shows a wide but shallow concavity in the middle, whereas the posterior margin forms the medial portion of the occipital

condyle. This bone fuses with the sphenoid and the elements-X anteriorly, the prootics anterolaterally and the otooccipitals posterolaterally.

SPHENOID

The unpaired sphenoid (Fig. 10K, M–O) is a subquadrangular and flattened bone, devoid of cristae ventrolaterales. The anterolaterally developed basipterygoid processes are very short, moderately wide, flat and subrectangular in ventral view; their distal end is slightly dorsoventrally enlarged and tilted at an angle of 30° in anterior view (Fig. 10K). Together with the lateral margins of the sphenoid, the basipterygoid processes define a laterally directed concavity along both lateral sides of the bone. The middle of the dorsal surface is smooth and flattened because of the absences of the crista sellaris, of a deep sella turcica and of the trabeculae cranii (Fig. 10N). A well-developed, wide laminar and triangular parasphenoid rostrum is present, projecting anteriorly between the basipterygoid processes. The Vidian canals pass through the lateral sides of the bone, opening anteriorly by the medial side of the basipterygoid processes, medially with a very anteroposteriorly elongated inner opening and posterolaterally by the contact with the prootics. The smooth ventral surface is crossed longitudinally by a wide sunken area (Fig. 10O). The posterior margin of the sphenoid is fused with the basioccipital medially and the prootics laterally. The elements-X cover ventrally the posterior half of the lateral margins of the bone.

ELEMENT-X

This paired bone contacts the anterolateral corner of the basioccipital and covers the posterolateral corner of the sphenoid. These elements have been interpreted as epiphyses for muscular attachment (Gans & Montero, 2008), but Montero *et al.* (2017) recently considered them to be basicranial sesamoids. Montero *et al.* (2017) also related these bones to ossifications present on the sphenooccipital tubercles in other squamates. In *Blanus*, each element-X is represented by a laminar and subovoid small bone (Fig. 11), which is usually fused completely with the surrounding elements (Fig. 10O).

SUPRAOCCIPITAL

The unpaired supraoccipital (Fig. 10K, L, N) is composed of a thin middle portion almost completely overlapped by the parietal and of two expanded lateral portions, which fuse with the prootic and the otooccipital. The bone has a rather flat general aspect. In dorsal view, its posterior margin is characterized

Figure 11. Close-up of the posterior half of the skull of *Blanus vandellii* (ZSM 175-1993-1), showing the unfused elements-X. Abbreviations: a, angular; bo, basioccipital; cb, compound bone; ex, element-X; oo, otooccipital; pa, palatine; pt, pterygoid; q, quadrate; sp, sphenoid; st, stapes; ts, tabulosphenoid. Scale bar: 1 mm.

by the presence of a deep and wide U-shaped notch (Fig. 10N). A strong and slightly dorsoventrally compressed processus ascendens is present. It projects for a short distance beyond the anterior margin, but it continues posteriorly on the dorsal surface with a distinct supraoccipital crest, reaching the posterior notch. The crest is not developed in juveniles (e.g. *B. vandellii* ZSM 175-1993-1 and 175-1993-2).

PROOTIC

The anterior portion of the bulge-like otic capsules is composed of the prootics (Fig. 10K, M–O). They are usually fused completely with the otooccipitals and the supraoccipital; therefore, their limits are not clearly recognizable. The alar process is long and triangular; it is wide by its base, but it narrows and tends to bend ventrally by its anterior end. The anterior inferior process is reduced and almost entirely occupied by the

fenestra ovalis, the anterior margin of which is marked by a moderately developed ridge. On the external surface of the bone, a wide facial foramen is visible anterior to the fenestra. A distinct crista prootica is absent. The alar and the anterior inferior processes define a very wide and U-shaped incisura prootica. Ventrally, the prootics contact the sphenoid and the basioccipital.

OTOOCCIPITAL

The posterior portion of the otic capsule is included in the otooccipital (Fig. 10L–O), which is made by the fusion of the exoccipital and the opisthotic. The otooccipital is usually fused completely with the prootic and the supraoccipital. It is also fused with the basioccipital ventrally, taking part in the formation of the occipital condyle. In posterior view, the wide vagus foramen is visible inside a wide cavity (Fig. 10L), the jugular foramen of Gans & Montero (2008). A variable number of small hypoglossal foramina flank the vagus foramen inside the concavity. The anterolaterally oriented paroccipital process is very poorly developed, represented only by a robust and ridge-like structure on the lateral surface of the otooccipital.

STAPES

The stapes is made up of a circular and very wide footplate and a very short shaft (Fig. 12).

DENTARY

The dentary (Figs 10P, Q, 13) has a moderately wide mandibular symphysis, which is anteroposteriorly inclined at an angle of ~45°. On the medial surface, the Meckelian fossa is represented by a very narrow

Figure 12. Close-up of the right stapes (indicated by the black arrow) in the skull of *Blanus vandellii* (ZSM 653-0-2). Scale bar: 1 mm.

groove running along the straight ventral margin of the bone. Dorsally, a high subdental ridge separates the fossa from the alveolar shelf, which bears subpleurodont, robust and canine-like teeth. The tooth crowns curve slightly posteromedially. The number of teeth is usually eight, but Bailon (1991) and Gans & Montero (2008) stated that sometimes there can be seven. This is also confirmed by some of the specimens studied here (e.g. *B. aporus* ZSM 37-1993-1, 37-1993-2 and 381-1976, *B. vandellii* ZSM 175-1993-1 and 175-1993-2, *B. mettetali* MCCI R-1182, the right dentaries of *B. vandellii* ZSM 652-0-1 and 653-0-1 and the left dentaries of *B. aporus* MCCI R-1680, ZMB 31155 and ZSM 264-1988-1 and *B. vandellii* ZSM 652-0-2 and 653-0-2). Seven is also the number of dentary tooth positions reported by Boulenger (1885) for *B. cinereus*. A small ninth tooth position was reported by Bolet *et al.* (2014) for a single specimen of *B. strauchi*. The right dentary of ZSM 264-1988-1 (*B. aporus*) also bears nine teeth. The alveolar canal, which houses the inferior alveolar nerve, is enclosed in the subdental ridge. This canal is narrow anteriorly, but widens posteriorly, opening near the posterior end of the dentary (posterior to the last tooth position) with a very wide posterior cavity. The intramandibular septum, which closes the canal ventrally, extends posteriorly with a pointed and slender portion, which is fused to the wall of the dentary (i.e. it is not free). Owing to the presence of the projection of the septum, the posterior end of the subdental ridge shows a wide V-shaped notch in medial view (Fig. 10P). Three processes are located by the posterior end of the bone. The superior and inferior posterior processes are well developed, wide and pointed. The superior posterior process projects posterodorsally, covering the lateral surface of the coronoid process of the coronoid. The inferior posterior process, in contrast, is developed in the posterior direction, covering ventrolaterally the anterior half of the compound bone. Between these two processes, there is a posteriorly directed, small and pointed central posterior process. This latter process, however, is lacking in ZSM 37-1993-1 and 37-1993-2, both corresponding to *B. aporus*. The lateral surface of the dentary is smooth, except for the presence of three wide mental foramina (five in the right dentary of *B. cinereus* ZSM 27-1988-2, four in both dentaries of *B. vandellii* ZSM 175-1993-1 and 227-1975 and in the left dentaries of *B. vandellii* ZSM 5482003 and *B. cinereus* ZSM 27-1988-1).

SPLENIAL

The splenial is an anteroposteriorly elongated, thin and very slender blade-like bone (Fig. 13). The anterior portion is slightly wider than the posterior one. A single foramen pierces the bone; it is located at midlength
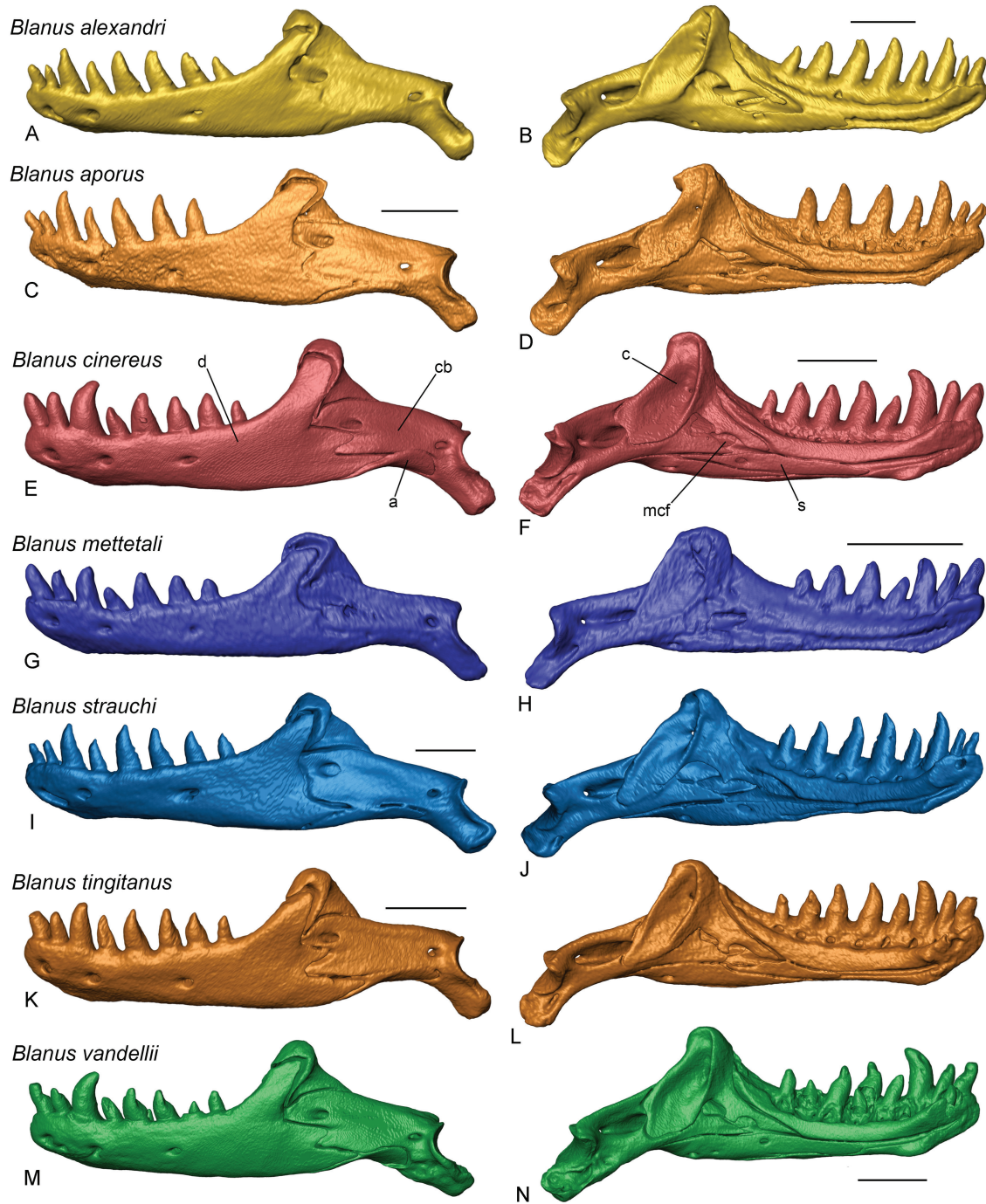
Figure 13. Left lower jaw of *Blanus* species in lateral (A, C, E, G, I, K, M) and medial (B, D, F, H, J, L, N) views. A–B, *Blanus alexandri* (MCCI R-1634). C–D, *Blanus aporus* (ZMB 14116). E–F, *Blanus cinereus* (ZSM 27-1988-1). G–H, *Blanus mettetali* (MCCI R-1182). I–J, *Blanus strauchi* (MCCI R-1635). K–L, *Blanus tingitanus* (MCCI R-1176). M–N, *Blanus vandellii* (ZSM 227-1975). Abbreviations: a, angular; c, coronoid; cb, compound bone; d, dentary; mcf, mandibular central foramen; s, splenial. Scale bars: 1 mm.

in *B. tingitanus* and slightly shifted posteriorly in *B. alexandri*, *B. aporus*, *B. cinereus*, *B. strauchi* and *B. vandellii*. It is not clear whether this foramen is the anterior inferior one or the anterior mylohyoid one.

We were not able to locate the splenial in the single specimen of *B. mettetali* examined, but this could be attributable to technical issues occurring in the scanning process owing to the ethanol preservation.

Coronoid

The coronoid (Figs 10R, S, 13) is thin and straight in dorsal view. In medial view, it is triradiate, with an anteromedial, a coronoid and a posteromedial processes. The anteroventrally developed anteromedial process is slender and pointed. A wide notch is present on its ventral margin, marking dorsally the mandibular central foramen. The dorsally developed coronoid process is moderately wide, subtriangular and has a rounded dorsal end. The wide articular surface with the superior posterior process of the dentary stands out on its lateral surface, bordered by a well-developed and arched ridge. The posteroventrally developed posteromedial process is wide, roughly leaf shaped and has a pointed distal end. Sometimes, the posterior margin of this process displays a more-or-less developed and posteriorly directed expansion (Fig. 13D, F, N). Both the presence/absence of this expansion and its degree of development differ intraspecifically and even between opposite coronoids of the same individual. On the medial surface of the bone, a moderately developed coronoid ridge runs vertically from the tip of the coronoid process to the ventral margin of the bone.

Angular

The angular is thin, laminar, very narrow and anteroposteriorly elongated (Fig. 13). It has a pointed anterior end, but widens posteriorly, ending with a rounded posterior end. Its posterior half is tilted at an angle of ~90° compared with the anterior one. This bone is pierced by a wide foramen at midlength.

Compound bone

The articular, prearticular and surangular are fused to form a short compound bone (Fig. 10T, U, 13), which encloses the posterior portion of Meckel's cartilage in a tubular structure. The dorsal margin is sharp and slightly convex, whereas the ventral one is straight in the anterior portion but becomes concave posteriorly because of the ventral bending of the retroarticular process. By the anterior end, the surangular (laterally) and the prearticular (medially) portions are still recognizable, given that they are not completely fused to one another. Both portions are pointed anteriorly, but the surangular projects beyond the prearticular in medial view (with the dentary process sensu Gans & Montero, 2008). The surangular portion presents a mediodorsally directed flattened area, which is covered by a dorsal laminar expansion of the prearticular portion. A wide, almost vertical and strongly concave articular condyle is present by the posterior end of the bone. Ventrally to it, the stocky, short and lobe-shaped retroarticular process projects posteroventrally. The retroarticular process is slightly concave dorsomedially and shows a moderately wide foramen for the chorda tympani on the medial surface, near its base. The size and the precise position of the foramen show minor individual variation, but it is invariably located by the base of the retroarticular process and ventrally to the articular condyle. The lateral surface of the retroarticular process is smooth. The lateral surface of the compound bone is also smooth, with only two wide foramina: the anterior surangular foramen, anterolaterally directed and located by the base of the dental process, and the posterior surangular one, laterally directed and located near the articular condyle. The ventral surface is covered by the narrow articular surface with the angular, which reaches the retroarticular process. In medial view, a moderately small adductor fossa stands out on the posterior half of the bone, anterior to the mandibular condyle.

DISCUSSION

Cranial morphology of extant *Blanus* species

Kearney (2003) and Gans & Montero (2008) considered the skull of *Blanus* to be reminiscent of the primitive morphological condition in amphisbaenians. This is attributable to the fact that *Blanus* lacks distinctively apomorphic features as seen in many other amphisbaenians, such as a pronounced craniofacial angle, a spade snout or a keeled snout. Additional primitive features of *Blanus* could be the less complicated contact between cranial elements and their small overlap compared with other amphisbaenians (e.g. Kearney *et al.*, 2005). Indeed, the skull of *Blanus* has a rather simple morphology compared with that of many other amphisbaenians and, to a certain extent, its overall shape recalls the capsule-like morphology of the skull of *Cryptolacerta hassiaca* Müller *et al.*, 2011, which is commonly considered to be related to the ancestor of the group (Müller *et al.*, 2011). This latter statement was recently questioned by Tałanda (2016), and Longrich *et al.* (2015) recovered *Cryptolacerta* as a lacertid. However, the position recovered by Longrich *et al.* (2015) might be linked with inaccurate scorings, and a revision of their analysis is in progress. Moreover, recent phylogenies (e.g. Müller *et al.*, 2011; Longrich *et al.*, 2015) failed to recover blanids as basal members of Amphisbaenia, a position that is instead occupied by the spade-snouted rhineurids. As such, it remains questionable if the skull of *Blanus* in fact represents a plesiomorphic morphology. This is also enhanced by the fact that the skull of *Slavoia darevksii*, recently proposed as a Late Cretaceous stem amphisbaenian by Tałanda (2016, 2017) based on several well-preserved specimens, clearly differs from that of *Blanus* in having a shorter and wider general shape. Additional fossils of

stem amphisbaenians and stem blanids are therefore needed to shed more light on the early evolutionary history of these clades.

Within *Blanus*, a homogeneous skull morphology is shared by all of the seven extant species of the genus. This morphological homogeneity most probably reflects similar life habits. The capsule-like morphology is typical of amphisbaenians that burrow by simple head ramming, in contrast to more complex digging techniques used by spade- or keeled-snouted worm lizards (Vitt & Caldwell, 2009). Leaving ontogenetic and minor individual variation aside, there are only a few main features that differ significantly among the different species. These are the anterior outline of the premaxilla (in both lateral and ventral views), the longitudinal depression on the anterodorsal surface of the premaxilla, the size of the premaxillary dentition, and the inner ridge on the quadrate.

The different degrees of anterior protrusion of the premaxilla are clearly recognizable in Bedriaga's (1884) drawings of the skulls of *B. cinereus* and *B. strauchi* (see also Bolet *et al.*, 2014; Kazi & Hipsley, 2018), and it is commonly reported in the field guides of European amphibians and reptiles as one of the few morphological characters that distinguish *B. strauchi* from the Iberian species, *B. cinereus* and *B. mariae* (*B. vandellii* and *B. cinereus*, respectively, after Ceríaco & Bauer, 2018) in the field (i.e. 'snout overhangs lower jaw'; Speybroeck *et al.*, 2016: 347; but see also Arnold & Ovenden, 2002). Indeed, it is interesting to note that the two different morphologies perfectly discriminate between the eastern and the western clades, with all eastern species showing an overhanging premaxilla and all western ones showing an anteriorly flat premaxilla. This confirms what was already suggested by Bolet *et al.* (2014) and might indicate that this character is of phylogenetic significance. Nevertheless, whether the plesiomorphic condition is represented by the flat morphology or by the overhanging outline is far from established. In any case, the different morphologies might be related to differences in prey capture and manipulation in the two clades, although other possible functional explanations cannot be excluded (linked, for example, to differences in burrowing techniques).

The shape of the anterior outline of the premaxilla in ventral view and the anterodorsal depression that is occasionally present on the same bone, in addition to the size of the premaxillary dentition in relationship to the teeth on the maxilla, also allow discrimination between the western and eastern species, although less easily. Regarding tooth size, the main issue is the overlap that sometimes occurs between specimens belonging to the two groups. Concerning the anterior outline in ventral view and the depression, the high variation displayed by the eastern species also includes morphologies (i.e. the most roundish premaxillae lacking a clear depression) that approach the condition seen in the Western Group. Nevertheless, identification of the bones based on these characters is possible in the presence of the extreme morphologies. Premaxillae hosting teeth that are either distinctly smaller or roughly of a similar size compared with the maxillary teeth can be assigned to the Eastern or Western Group, respectively. Bones that show either a distinctly squared anterior outline or a deep depression can be referred to the Eastern Group.

A similar agreement between the molecular-based clades and the morphological patterns is not present in the case of the inner ridge of the quadrate, i.e. the distribution of the three different degrees of development of this ridge does not match the relationships between *Blanus* species as reported by Sindaco *et al.* (2014) and Sampaio *et al.* (2015). This is particularly evident in the Western Group, with *B. vandellii* sharing a virtually absent ridge with *B. mettetali* instead of having a low ridge as seen in its sister taxon, *B. cinereus*. The latter species, in contrast, shares its condition with *B. tingitanus* and, even more surprisingly, with the eastern species *B. alexandri*. This issue appears less complicated in the Eastern Group, in which *B. alexandri* is the only species with a low ridge. Given that the phylogenetic analysis reported by Sindaco *et al.* (2014) recovered *B. alexandri* and *B. aporus* as sister taxa in a clade that is sister to *B. strauchi*, it might be possible that the relatively stronger development of the ridge represents the plesiomorphic condition in the Eastern Group and that the condition shown by *B. alexandri* is a parallel but autapomorphic feature of this species. The pattern displayed by the Western Group might then be explained by multiple convergences. Nevertheless, these hypotheses should be treated with caution until they are tested by means of a comparative phylogenetic analysis, particularly if one also takes into account that some species are underrepresented in our sample.

TAXONOMIC AFFINITIES OF *BLANUS* FOSSILS

European fossil amphisbaenians are rather abundant and clearly show a progressive southward range contraction in addition to a former continuous range that included both the Apennine and the Balkan peninsulas, and some of their major islands (Estes, 1983; Roček, 1984; Schleich, 1985; Cavallo *et al*, 1993; Augé & Rage, 1995, 2000; Delfino, 1997, 2002, 2003; Böhme, 1999a, b, 2010; Delfino & Bailon, 2000; Abbazzi *et al.*, 2004; Augé, 2005, 2012; Venczel & Sanchiz, 2006; Blain, 2009; Čerňanský & Venczel, 2011; Delfino *et al.*, 2011; Bolet & Evans, 2013; Folie *et al.*, 2013; Bolet *et al.*, 2014; Colombero *et al.*, 2014, 2017; Čerňanský *et al.*, 2015a, b; Rage & Augé, 2015;

Georgalis *et al.*, 2016, 2018b; Bolet, 2017). However, they are frequently represented by isolated vertebrae that are not considered diagnostic even at the family rank (Estes, 1983; rhineurid vertebrae might be a notable exception) and therefore a precise taxonomic identification of European fossil remains of these squamates is often impossible.

Nevertheless, there are a few exceptions, the most significant of which is the almost complete skull of *B. mendezi* found in middle/late Miocene (10.6 Ma) sediments at Abocador de Can Mata (NE Iberian Peninsula; Bolet *et al.*, 2014). *Blanus mendezi* differs from other *Blanus* species in the larger size and in a number of skull characters, as well as in a few vertebral characters (see Bolet *et al.*, 2014, for a differential diagnosis of the species). The premaxilla of *B. mendezi* has a flat anterior outline in lateral view, a rounded anterior shape in ventral view, and teeth that are not distinctly smaller than those of the maxilla, similar to extant species of the Western Group. The quadrates, in contrast, resemble some species of the Eastern Group (i.e. *B. aporus* and *B. strauchi*) in the distinct development of the inner ridge. This may lead to some possible assumptions. First, *B. mendezi* might be related closely to the Western Group of *Blanus*, because of the morphological features of the premaxilla, and the distinct inner ridge might be a plesiomorphic character not only for the Eastern Group (see above), but for the genus *Blanus* as a whole. Second, *B. mendezi* might be a basal member of the Eastern Group, so that the flat morphology of the premaxilla would be the plesiomorphic feature. Bolet *et al.* (2014) considered *B. mendezi* as sister to all extant members of the western clade, but subsequently the species was recovered in a polytomy with *B. strauchi* and *B. antiquus* by Longrich *et al.* (2015). It appears therefore clear that the phylogenetic relationships of *B. mendezi* are still a matter of debate, also taking into account the contrasting information provided by the two morphological characters considered herein.

No quadrates are known for the other extinct species of *Blanus*, and only the type material of *B. antiquus* includes a premaxilla. Schleich (1985) stated that this single premaxilla is more similar to those of *B. strauchi* available to him for study, rather than to those of *B. cinereus*. However, it is not possible to evaluate the morphology of the anterior outline of the bone from the description and figures provided by this author, and therefore we are unable to confirm this statement based on our observations. It is interesting to note that the supposed premaxilla of *B. cinereus* (most probably *B. vandellii* following Ceríaco & Bauer, 2018, given that Schleich's specimen comes from Almería, in south-eastern Spain) figured by Schleich (1985) does not look like amphisbaenian premaxillae at all, displaying a morphology that would fit more with a lacertid lizard, for example (Bolet *et al.*, 2014). If the premaxilla he used as a comparison did not in fact belong to *B. cinereus*, this might have been the main reason behind his idea of the premaxilla of *B. antiquus* being more similar to that of *B. strauchi*.

Type cranial remains of *B. gracilis* (originally described as *Omoiotyphlops gracilis* by Roček, 1984) and *B. thomaskelleri* include only dentaries. Roček (1984) himself pointed out the affinities of the former species with *Blanus*, of which the genus *Omoiotyphlops* was later considered a junior synonym (Estes, 1983; Augé & Rage, 1995, 2000; Delfino, 1997). The affinities of *B. gracilis* within the genus *Blanus* are not clear, although Bolet *et al.* (2014) included this species in the Eastern Group together with *B. strauchi*. Venczel & Ştiucă (2008) tentatively assigned a small premaxilla from Tauţ (Romania) to *Blanus* cf. *gracilis*. If this identification is correct, *B. gracilis* had an anteriorly flat premaxilla. This might be supported further by the presence of a similar premaxilla found in Dolnice (Czech Republic), the type locality of *B. gracilis*, which was assigned to an indeterminate squamate by Roček (1984), but might be attributed to *B. gracilis* according to Venczel & Ştiucă (2008). Another isolated premaxilla attributed to *B. gracilis* was reported by Venczel & Sanchiz (2006) from Oschiri (Italy) but has never been described or figured. If the phylogenetic position of *B. gracilis* assumed by Bolet *et al.* (2014) proves to be correct, the Romanian specimen could support the hypothesis that the flat premaxilla is the condition displayed by the common ancestor of both the Western and Eastern Groups, being replaced later by the overhanging morphology in extant eastern species. Nevertheless, either convergent evolution or an alternative position of *B. gracilis* in the Western Group must be considered as possible alternative explanations. Moreover, some authors (Böhme, 1999b; Augé & Rage, 2000) proposed the synonymy of *B. gracilis* with *B. antiquus*, although their status as distinct species is supported by some differences in the morphology of the dentary (Bolet *et al.*, 2014).

The possible affinities of *B. thomaskelleri* are even more difficult to assess, owing to the fact that this species is represented by only two isolated and incompletely preserved dentaries (Čerňanský *et al.*, 2015b). The main diagnostic feature of this species is a short superior posterior process that does not project distinctly in the dorsal direction (Čerňanský *et al.*, 2015b), a peculiar feature that is unknown in any other *Blanus* species, either extant or extinct. Nevertheless, *B. thomaskelleri* might represent a key point in understanding the early evolution of *Blanus*, given that it figures as one of the oldest *Blanus* species known; its two fossil remains have been found in German and Czech early Miocene sites (Mammal Neogene units MN 2 to MN 3;

Čerňanský & Venczel, 2011; Čerňanský *et al.*, 2015b), with only *B. gracilis* possibly coming from roughly coeval sediments as the oldest fossil of *B. thomaskelleri* (fossils from the lower Miocene of Oschiri, in Sardinia, reported, but not described, by Venczel & Sanchiz, 2006). The finding of new material confidently attributable to *B. thomaskelleri*, in particular either premaxillae or quadrates, would therefore be of utmost significance for deciphering further the internal phylogeny of the genus.

Georgalis *et al.* (2018a) recently referred a fragmentary dentary from the Miocene of Turkey to the *Blanus strauchi* complex. This attribution is based on both a biogeographical rationale and morphological comparisons. Morphological features used to exclude affinities of this specimen with the Western Group (represented by *B. cinereus*) include a different tooth morphology, larger interdental gaps and a Meckelian fossa that appears wider posteriorly. However, as already noted by the authors themselves, these features might simply represent minor variation within blanids, which is apparently confirmed by the variation displayed by the dentaries of the various *Blanus* species depicted in Figures 10 and 13. The present study shows that tooth shape is highly variable even in a single *Blanus* dentary (e.g. Fig. 13F), that large interdental gaps can also be present in western species (e.g. *B. cinereus*; Fig. 13F), and that a Meckelian fossa that does not distinctly widen posteriorly is also present in *B. strauchi* (Fig. 10P). Moreover, the low diagnostic value of *Blanus* dentaries appears to be confirmed by our morphological comparisons, at least as far as extant species are concerned.

The morphological differences highlighted in our comparative analysis also provide useful information for assessing the affinities of fossil remains that are assigned to genera other than *Blanus* but considered closely related to it. This is the case, for example, in an isolated premaxilla from the late Miocene of Cava Rodisano (Gargano 'Terre Rosse', Italy), which was attributed to *Palaeoblanus* owing to its association with dentary remains that show the diagnostic characters of this genus (Delfino, 2002, 2003). This premaxilla has a flat (in lateral view) and rounded (in ventral view) anterior outline, with no anterodorsal depression, and its general morphology is fully comparable to that of extant western species of *Blanus*, which means that the premaxilla should either be assigned to *Blanus* or that the flat morphology of this bone is shared by *Blanus* and *Palaeoblanus*. Hoverver, it should be noted that the taxonomic validity of *Palaeoblanus* was recently questioned by Čerňanský *et al.* (2016), and a thorough revision of all the fossils assigned to the latter genus is needed before reaching a more definitive conclusion on this issue.

CONCLUSIONS

Amphisbaenians of the genus *Blanus* share a rather homogeneous skull morphology. As a result, identification at the species level based on isolated bones is often difficult. Only the premaxilla and quadrate display informative features that allow discrimination among the different species. Nevertheless, clear diagnostic osteological features of single *Blanus* species are still unknown. As far as the extant species are concerned, the morphology of the anterior outline of the premaxilla in lateral view is particularly significant in discriminating between the two main clades as they are recognized in molecular phylogenies. A more complicated pattern is shown by the degree of development on the inner ridge present on the quadrate. In this case, it might be required to hypothesize multiple convergences to explain the presence of similar morphologies in species that are supposed to be related distantly.

In spite of this inability to identify remains precisely at the species level, new diagnostic features, such as the ones detected in the present study, are potentially useful to provide a more accurate taxonomic attribution of fossil specimens and to discern the deep-time evolutionary history of European blanids. This is particularly important given that, even when their remains are assigned to particular genera or species, the phylogenetic relationships of European extinct amphisbaenians relative to their extant counterparts are often unclear. The extinct *B. mendezi*, for example, displays a premaxilla that resembles the Western Group in its morphology, but also a distinct inner ridge on the quadrate like most species of the Eastern Group. Future analyses of these and other morphological features in a rigorous cladistic framework will hopefully help to clarify the phylogenetic relationships between extinct and living blanids.

REFERENCES

Abbazzi L, **Angelone C**, **Arca M**, **Barisone G**, **Bedetti C**, **Delfino M**, **Kotsakis T**, **Marcolini F**, **Palombo MR**, **Pavia M**, **Piras P**, **Rook L**, **Torre D**, **Tuveri C**, **Valli AMF**, **Wilkens B. 2004.** Plio-Pleistocene fossil vertebrates of Monte Tuttavista (Orosei, Eastern Sardinia, Italy), an overview. *Rivista Italiana di Paleontologia e Stratigrafia* **110:** 681–706.

Albert EM, **Fernández A. 2009.** Evidence of cryptic speciation in a fossorial reptile: description of a new species of *Blanus* (Squamata: Amphisbaenia: Blanidae) from the Iberian Peninsula. *Zootaxa* **2234:** 56–68.

Arnold N, **Ovenden D. 2002.** *A field guide to the reptiles and amphibians of Britain and Europe*. London: Harper Collins.

Augé ML. 2005. Évolution des lézards du Paléogène en Europe. *Mémoires du Muséum National d'Histoire Naturelle* **192:** 1–369.

Augé M. 2012. Amphisbaenians from the European Eocene: a biogeographical review. *Palaeobiodiversity and Palaeoenvironments* **92:** 425–443.

Augé M, **Rage J-C. 1995.** Le Garouillas et les sites contemporains (Oligocene, MP 25) des Phosphorites du Quercy (Lot, Tarn-et-Garonne, France) et leurs faune de vertébrés. 2. Amphibiens et Squamates. *Palaeontographica Abteilung A* **236:** 11–32.

Augé M, **Rage J-C. 2000.** Les Squamates (Reptilia) du Miocéne moyen de Sansan. *Mémoires du Muséum National d'Histoire Naturelle* **183:** 263–313.

Bailon S. 1991. *Amphibiens et reptiles du Pliocène et du Quaternaire de France et d'Espagne: mise en place et evolution des faunes*. Unpublished D. Phil. Thesis, Université Paris VII.

Bedriaga J. 1884. *Amphisbaena cinerea* Vand. und *A. strauchi* v. Bedr. Erster Beitrag zur Kenntniss der Doppelschleichen. *Archiv für Naturgeschichte* **50:** 23–77.

Blain H-A. 2009. Contribution de la paléoherpétofaune (Amphibia & Squamata) à la connaissance de l'évolution du climat et du paysage du Pliocène supérieur au Pléistocène moyen d'Espagne. *Treballs del Museu de Geologia de Barcelona* **16:** 39–170.

Böhme M. 1999a. Die miozäne Fossil-Lagerstätte Sandelzhausen. 16. Fisch-und Herpetofauna – Erste Ergebnisse. *Neues Jahrbuch für Geologie und Paläontologie, Abhandlungen* **214:** 487–496.

Böhme M. 1999b. Doppelschleichen (Sauria, Amphisbaenidae) aus dem Untermiozän von Stubersheim 3 (Süddeutschland).

Mitteilungen der Bayerischen Staatssammlung für Paläontologie und Historische Geologie **39:** 85–90.

Böhme M. 2010. Ectothermic vertebrates (Actinopterygii, Allocaudata, Urodela, Anura, Crocodylia, Squamata) from the Miocene of Sandelzhausen (Germany, Bavaria) and their implications for environment reconstruction and palaeoclimate. *Paläontologische Zeitschrift* **84:** 3–41.

Bolet A. 2017. First early Eocene lizards from Spain and a study of the compositional changes between late Mesozoic and early Cenozoic Iberian lizard assemblages. *Palaeontologia Electronica* **20:** 20A.

Bolet A, **Delfino M**, **Fortuny J**, **Almécija S**, **Robles JM**, **Alba DM. 2014.** An amphisbaenian skull from the European Miocene and the evolution of Mediterranean worm lizards. *PLoS One* **9:** e98082.

Bolet A, **Evans SE. 2013.** Lizards and amphisbaenians (Reptilia, Squamata) from the late Eocene of Sossís (Catalonia, Spain). *Palaeontologia Electronica* **16:** 8A.

Bons J. 1963. Notes sur *Blanus cinereus* (Vandelli). Description d'une sous-espèce Marocaine: *Blanus cinereus mettetali* ssp. nov. *Bulletin de la Société des Sciences Naturelles et Physiques du Maroc* **43:** 95–107.

Boulenger GA. 1885. *Catalogue of the lizards in the British Museum (Natural History)*. London: The Trustees of the British Museum.

Busack SD. 1988. Biochemical and morphological differentiation in Spanish and Moroccan populations of *Blanus* and the description of a new species from northern Morocco (Reptilia, Amphisbaenia, Amphisbaenidae). *Copeia* **1988:** 101–109.

Cavallo O, **Sen S**, **Rage J-C**, **Gaudant J. 1993.** Vertébrés messiniens du faciès a congéries de Ciabòt Cagna, Corneliano d'Alba (Piémont, Italie). *Rivista Piemontese di Storia Naturale* **14:** 3–22.

Ceríaco LMP, **Bauer AM. 2018.** An integrative approach to the nomenclature and taxonomic status of the genus *Blanus* Wagler, 1830 (Squamata: Blanidae) from the Iberian Peninsula. *Journal of Natural History* **52:** 849–880.

Čerňanský A, **Augé ML**, **Rage J-C. 2015a.** A complete mandible of a new amphisbaenian reptile (Squamata, Amphisbaenia) from the late middle Eocene (Bartonian, MP 16) of France. *Journal of Vertebrate Paleontology* **35:** e902379.

Čerňanský A, **Klembara J**, **Müller J. 2016.** The new rare record of the late Oligocene lizards and amphisbaenians from Germany and its impact on our knowledge of the European terminal Palaeogene. *Palaeobiodiversity and Palaeoenvironments* **96:** 559–587.

Čerňanský A, **Rage J-C**, **Klembara J. 2015b.** The early Miocene squamates of Amöneburg (Germany): the first stages of modern squamates in Europe. *Journal of Systematic Palaeontology* **13:** 97–128.

Čerňanský A, **Venczel M. 2011.** An amphisbaenid reptile (Squamata, Amphisbaenidae) from the lower Miocene of Northwest Bohemia (MN 3, Czech Republic). *Neues Jahrbuch für Geologie und Paläontologie-Abhandlungen* **260:** 73–77.

Colombero S, **Alba DM**, **D'Amico C**, **Delfino M**, **Esu D**, **Giuntelli P**, **Harzhauser M**, **Mazza PPA**, **Mosca M**,

Neubauer TA, **Pavia G**, **Pavia M**, **Villa A**, **Carnevale G. 2017.** Late Messinian mollusks and vertebrates from Moncucco Torinese, north-western Italy. Paleoecological and paleoclimatological implications. *Palaeontologia Electronica* **20:** 10A.

Colombero S, **Angelone C**, **Bonelli E**, **Carnevale G**, **Cavallo O**, **Delfino M**, **Giuntelli P**, **Mazza P**, **Pavia G**, **Pavia M**, **Repetto G. 2014.** The upper Messinian assemblages of fossil vertebrate remains of Verduno (NW Italy): another brick for a latest Miocene bridge across the Mediterranean. *Neues Jahrbuch für Geologie und Paläontologie-Abhandlungen* **272:** 287–324.

Conrad JL. 2008. Phylogeny and systematics of Squamata (Reptilia) based on morphology. *Bulletin of the American Museum of Natural History* **310:** 1–182.

Delfino M. 1997. *Blanus* from the Early Pleistocene of Southern Italy: another small tessera from a big mosaic. In: Böhme W, Bischoff W, Ziegler T, eds. *Herpetologia Bonnensis*. Bonn: Societas Europaea Herpetologica, 89–97.

Delfino M. 2002. *Erpetofaune italiane del Neogene e del Quaternario*. Unpublished D. Phil. Thesis, Università degli Studi di Modena e Reggio Emilia.

Delfino M. 2003. A Pleistocene amphisbaenian from Sicily. *Amphibia-Reptilia* **24:** 407–414.

Delfino M, **Bailon S. 2000.** Early Pleistocene herpetofauna from Cava dell'Erba and Cava Pirro (Apulia, Southern Italy). *Herpetological Journal* **10:** 95–110.

Delfino M, **Bailon S**, **Pitruzzella G. 2011.** The late Pliocene amphibians and reptiles from "Capo Mannu D1 Local Fauna" (Mandriola, Sardinia, Italy). *Geodiversitas* **33:** 357–382.

Estes R. 1983. *Handbuch der Paläoherpetologie 10A. Sauria terrestria, Amphisbaenia*. München: Friedrich Pfeil.

Evans SE. 2008. The skull of lizards and tuatara. In: Gans C, Gaunt A, eds. *Biology of the Reptilia*. Ithaca: Society for the Study of Amphibians and Reptiles, 1–347.

Folie A, **Smith R**, **Smith T. 2013.** New amphisbaenian lizards from the early Paleogene of Europe and their implications for the early evolution of modern amphisbaenians. *Geologica Belgica* **16:** 227–235.

Gans C, **Montero R. 2008.** An atlas of amphisbaenian skull anatomy. In: Gans C, Gaunt A, Adler K, eds. *Biology of the Reptilia. Volume 21. Morphology I. The skull and appendicular locomotor apparatus of Lepidosauria*. Ithaca: Society for the Study of Amphibians and Reptiles, 621–738.

Gauthier JA, **Kearney M**, **Maisano JA**, **Rieppel O**, **Behlke ADB. 2012.** Assembling the squamate tree of life: perspectives from the phenotype and the fossil record. *Bulletin of the Peabody Museum of Natural History* **53:** 3–308.

Georgalis GL, **Halaçlar K**, **Mayda S**, **Kaya T**, **Ayaz D. 2018a.** First fossil find of the *Blanus strauchi* complex (Amphisbaenia, Blanidae) from the Miocene of Anatolia. *Journal of Vertebrate Paleontology* **38:** e1437044.

Georgalis GL, **Villa A**, **Delfino M. 2018b.** The last amphisbaenian (Squamata) from continental Eastern Europe. *Annales de Paléontologie* **104:** 155–159.

Georgalis GL, **Villa A**, **Vlachos E**, **Delfino M. 2016.** Fossil amphibians and reptiles from Plakias, Crete: a glimpse into the earliest late Miocene herpetofaunas of southeastern Europe. *Geobios* **49:** 433–444.

Gervais P. 1853. Recherches sur l'ostéologie de plusieurs espèces d'Amphisbènes, et remarques sur la classification de ces reptiles. *Annales des Sciences Naturelles* **19–20:** 293–312.

Jollie MT. 1960. The head skeleton of the lizard. *Acta Zoologica* **41:** 1–64.

Kazi S, **Hipsley CA. 2018.** Conserved evolution of skull shape in Caribbean head-first burrowing worm lizards (Squamata: Amphisbaenia). *Biological Journal of the Linnean Society*. **125:** 14–29.

Kearney M. 2002. Appendicular skeleton in amphisbaenians (Reptilia: Squamata). *Copeia* **2002:** 719–738.

Kearney M. 2003. Systematics of the Amphisbaenia (Lepidosauria: Squamata) based on morphological evidence from recent and fossil forms. *Herpetological Monographs* **17:** 1–74.

Kearney M, **Maisano JA**, **Rowe T. 2005.** Cranial anatomy of the extinct amphisbaenian *Rhineura hatcherii* (Squamata, Amphisbaenia) based on high-resolution X-ray computed tomography. *Journal of Morphology* **264:** 1–33.

Longrich NR, Vinther J, Pyron RA, Pisani D, Gauthier JA. 2015. Biogeography of worm lizards (Amphisbaenia) driven by end-Cretaceous mass extinction. *Proceedings of the Royal Society B* **282:** 20143034.

Montero R, **Daza JD**, **Bauer AM**, **Abdala V. 2017.** How common are cranial sesamoids among squamates? *Journal of Morphology* **278:** 1400–1411.

Müller J, **Hipsley CA**, **Head JJ**, **Kardjilov N**, **Hilger A**, **Wuttke M**, **Reisz RR. 2011.** Eocene lizard from Germany reveals amphisbaenian origins. *Nature* **473:** 364–367.

Müller J, **Hipsley CA**, **Maisano JA. 2016.** Skull osteology of the Eocene amphisbaenian *Spathorhynchus fossorium* (Reptilia, Squamata) suggests convergent evolution and reversals of fossorial adaptations in worm lizards. *Journal of Anatomy* **229:** 615–630.

Rage J-C, **Augé M. 2015.** Valbro: a new site of vertebrates from the early Oligocene (MP 22) of France (Quercy). III - Amphibians and squamates. *Annales de Paléontologie* **101:** 29–41.

Reeder TW, **Townsend TM**, **Mulcahy DG**, **Noonan BP**, **Wood PL Jr**, **Sites JW Jr**, **Wiens JJ. 2015.** Integrated analyses resolve conflicts over squamate reptile phylogeny and reveal unexpected placements for fossil taxa. *PLoS One* **10:** e0118199.

Renous S, **Gasc JP**, **Raynaud A. 1991.** Comments on the pelvic appendicular vestiges in an amphisbaenian: *Blanus cinereus* (Reptilia, squamata). *Journal of Morphology* **209:** 23–38.

Roček Z. 1984. Lizards (Reptilia: Sauria) from the lower Miocene locality Dolnice (Bohemia, Czechoslovakia). *Rozpravy Československé Akademie Věd* **94:** 1–69.

Sampaio FL, **Harris DJ**, **Perera A**, **Salvi D. 2015.** Phylogenetic and diversity patterns of *Blanus* worm lizards (Squamata: Amphisbaenia): insights from mitochondrial and nuclear gene genealogies and species tree. *Journal of Zoological Systematics and Evolutionary Research* **53:** 45–54.

Schleich HH. 1985. Neue Reptilienfunde aus dem Tertiär Deutschlands 3. Erstnachweis von Doppelschleichen (*Blanus antiquus* sp. nov.) aus dem Mittelmiozän Süddeutschlands. *Münchner Geowissenschaftliche Abhandlungen* **4:** 1–16.

Sindaco R, **Jeremčenko VK. 2008.** *The reptiles of the Western Palearctic. 1. Annotated checklist and distribution atlas of the turtles, crocodiles, amphisbaenians and lizards of Europe, North Africa, Middle East and Central Asia*. Latina: Edizioni Belvedere.

Sindaco R, **Kornilios P**, **Sacchi R**, **Lymberakis P. 2014.** Taxonomic reassessment of *Blanus strauchi* (Bedriaga, 1884) (Squamata: Amphisbaenia: Blanidae), with the description of a new species from southeast Anatolia (Turkey). *Zootaxa* **3795:** 311–326.

Speybroeck J, **Beukema W**, **Bok B**, **Van Der Voort J**, **Velikov I. 2016.** *Field guide to the amphibians and reptiles of Britain and Europe*. London & New York: Bloomsbury.

Tałanda M. 2016. Cretaceous roots of the amphisbaenian lizards. *Zoologica Scripta* **45:** 1–8.

Tałanda M. 2017. Evolution of postcranial skeleton in worm lizards inferred from its status in the Cretaceous stem-amphisbaenian *Slavoia darevskii*. *Acta Palaeontologica Polonica* **62:** 9–23.

Tuniz C, **Bernardini F**, **Cicuttin A**, **Crespo ML**, **Dreossi D**, **Gianoncelli A**, **Mancini L**, **Mendoza Cuevas A**, **Sodini N**, **Tromba G**, **Zanini F**, **Zanolli C. 2013.** The ICTP-Elettra X-ray laboratory for cultural heritage and archaeology. *Nuclear Instruments and Methods in Physics Research Section A: Accelerators, Spectrometers, Detectors and Associated Equipment* **711:** 106–110.

Uetz P, **Freed P**, **Hošek J. 2017.** *The reptile database*. http://www.reptile-database.org

Vandelli D. 1797. Florae et faunae Lusitanicae specimen. *Memórias da Academia das Ciências de Lisboa* **1:** 37–79.

Venczel M, **Sanchíz B. 2006.** Lower Miocene amphibians and reptiles from Oschiri (Sardinia, Italy). *Hantkeniana* **5:** 72–75.

Venczel M, **Ştiucă E. 2008.** Late middle Miocene amphibians and squamate reptiles from Tauţ, Romania. *Geodiversitas* **30:** 731–763.

Vitt LJ, **Caldwell JP. 2009.** *Herpetology. An introductory biology of amphibians and reptiles, 3rd edn*. Burlington: Academic Press.

Wagler J. 1830. *Natürliches System der Amphibien, mit vorangehender Classification der Säugthiere und Vogel. Ein Beitrag zur vergleichenden Zoologie*. München, Stuttgart and Tübingen: J.G. Cotta.

Werner F. 1898. Über einige neue Reptilien und einen neuen Frosch aus dem cilicischsen Taurus. *Zoologische Anzeiger* **21:** 217–223.

Zangerl R. 1944. Contribution to the osteology of the skull of the Amphisbaenidae. *American Midland Naturalist* **31:** 417–454.

Zangerl R. 1945. Contributions to the osteology of the post-cranial skeleton of the Amphisbaenidae. *American Midland Naturalist* **33:** 764–780.

SUPPORTING INFORMATION

Additional Supporting Information may be found in the online version of this article at the publisher's web-site.

Table S1. List of studied specimens and related measurements.
Table S2. X-Ray computed microtomography scan parameters, 'Abdus Salam' International Centre of Theoretical Physics.
Table S3. X-Ray computed microtomography scan parameters, Museum für Naturkunde Berlin.